Cell Reports

Article

Transient splicing inhibition causes persistent DNA damage and chemotherapy vulnerability in triple-negative breast cancer

Graphical abstract

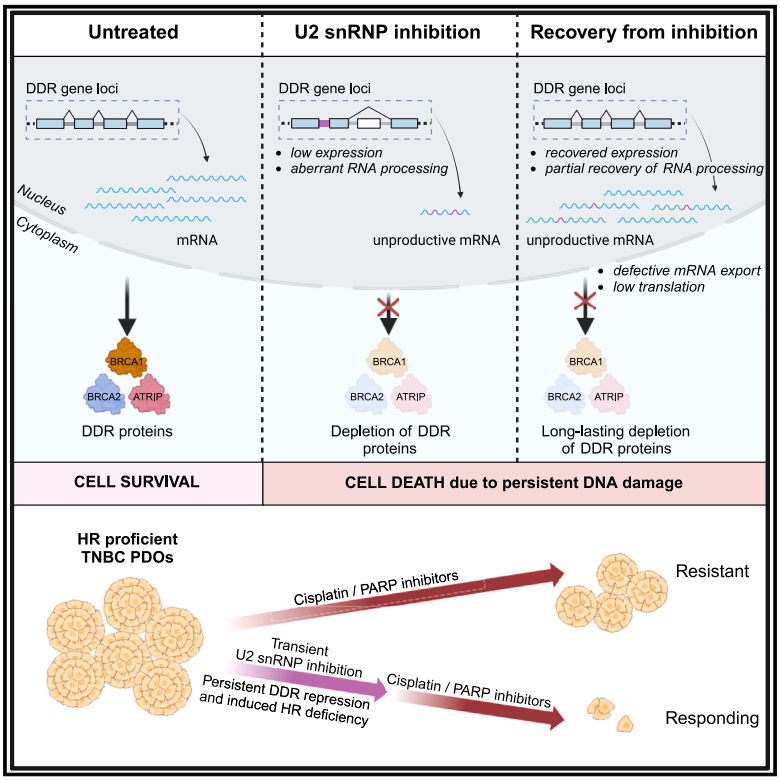

Highlights

- Inhibition of the U2 snRNP represses the DNA damage response pathway
- A transient splicing inhibition causes persistent DNA damage in TNBC
- U2 snRNP inhibition generates long-lasting depletion of DNA repair factors
- A pulse of splicing inhibition enhances the efficacy of DNA-damaging chemotherapy

Authors

Cinzia Caggiano, Valerio Petrera, Miriana Ferri, ..., Riccardo Masetti, Chiara Naro, Claudio Sette

Correspondence

cinzia.caggiano@unicatt.it (C.C.), claudio.sette@unicatt.it (C.S.)

In brief

Caggiano et al. report that short-term U2 snRNP inhibition elicits transient splicing defects while inducing long-lasting depletion of DNA repair factors, causing persistent DNA damage in genomically unstable triple-negative breast cancer. Pulsed inhibition of splicing mimics a sustained BRCAness condition and is a promising therapeutic strategy to overcome chemotherapy resistance.

Caggiano et al., 2024, Cell Reports *43*, 114751
September 24, 2024
https://doi.org/10.1016/j.celrep.2024.114751

CellPress

Cell Reports

CellPress
OPEN ACCESS

Article

Transient splicing inhibition causes persistent DNA damage and chemotherapy vulnerability in triple-negative breast cancer

Cinzia Caggiano,[1,2,*] Valerio Petrera,[1] Miriana Ferri,[1] Marco Pieraccioli,[2] Eleonora Cesari,[2] Alba Di Leone,[3] Martin Alejandro Sanchez,[3] Alessandra Fabi,[3] Riccardo Masetti,[3] Chiara Naro,[1,2] and Claudio Sette[1,2,4,*]

[1]Department of Neuroscience, Section of Human Anatomy, Catholic University of the Sacred Heart, Largo Francesco Vito 1, 00168 Rome, Italy

[2]GSTeP Organoids Research Core Facility, Fondazione Policlinico Universitario Agostino Gemelli IRCCS, Largo Agostino Gemelli, 00168 Rome, Italy

[3]Breast Unit, Department of Women, Children and Public Health Sciences, Fondazione Policlinico Universitario Agostino Gemelli IRCCS, 00168 Roma, Italy

[4]Lead contact

*Correspondence: cinzia.caggiano@unicatt.it (C.C.), claudio.sette@unicatt.it (C.S.)

https://doi.org/10.1016/j.celrep.2024.114751

SUMMARY

Triple negative breast cancer (TNBC) is an aggressive type of breast cancer. While most TNBCs are initially sensitive to chemotherapy, a substantial fraction acquires resistance to treatments and progresses to more advanced stages. Here, we identify the spliceosome U2 small nuclear ribonucleoprotein particle (snRNP) complex as a modulator of chemotherapy efficacy in TNBC. Transient U2 snRNP inhibition induces persistent DNA damage in TNBC cells and organoids, regardless of their homologous recombination proficiency. U2 snRNP inhibition pervasively deregulates genes involved in the DNA damage response (DDR), an effect relying on their genomic structure characterized by a high number of small exons. Furthermore, a pulse of splicing inhibition elicits long-lasting repression of DDR proteins and enhances the cytotoxic effect of platinum-based drugs and poly(ADP-ribose) polymerase inhibitors (PARPis) in multiple TNBC models. These findings identify the U2 snRNP as an actionable target that can be exploited to enhance chemotherapy efficacy in TNBCs.

INTRODUCTION

Although the development of new diagnostic, prognostic, and therapeutic tools has positively affected the life expectancy of breast cancer (BC) patients, this cancer still displays a relatively high lethality rate.[1,2] BC can be classified in subtypes that differ in histopathological and molecular features. Importantly, the identification of molecular drivers of BC subtypes has guided the development of highly efficacious targeted treatments. Most BCs (~70%) express the estrogen (ER^+) and progesterone receptor (PR^+), and these patients benefit from anti-estrogenic therapies.[1,2] Other BCs (~15%) feature amplification of the human epidermal growth factor receptor 2 ($HER2^+$) gene and are treated with antibodies and/or inhibitors for this receptor.[1,2] By contrast, triple-negative BCs (TNBCs; ~15%) are characterized by lack of expression of these receptors and display a higher tendency to relapse and worse clinical outcome,[3] thus representing a disproportionate fraction of BC-related deaths.

Chemotherapy is the main option for TNBC. However, these tumors often acquire resistance to treatments.[2,3] TNBCs are characterized by high heterogeneity with morphologically distinct subtypes (basal like, mesenchymal, and luminal androgen receptor positive) that are associated with different clinical courses.[4] However, an emerging common feature of TNBCs is the high frequency of mutations in DNA damage response (DDR) genes, which are associated with increased sensitivity to genotoxic stress and immunotherapies.[3,5] BRCA1 and BRCA2 are key proteins in the pathway that promotes DNA repair through homologous recombination (HR), a mechanism that ensures low mutation rates.[6] Cells harboring mutations in the *BRCA1/2* genes are HR deficient (HRD), display higher rates of genomic instability (GI), and are sensitive to inhibitors of alternative DNA repair pathways, such as poly(ADP-ribose) polymerase inhibitors (PARPi).[6] PARPi as monotherapy, or in combination with chemotherapy, have been shown to improve progression-free survival in HRD patients.[3] However, recent data in BRCA-mutant BCs indicate that treatment with PARPi as single agents failed to improve overall survival.[7,8] Moreover, a substantial fraction of TNBCs are HR proficient (HRP) and do not currently benefit from PARPi therapy. Thus, identification of mechanisms that promote DNA repair efficiency in HRP TNBCs may uncover targetable vulnerabilities that can be exploited to enhance the long-term effects of chemotherapy also

in patients that do not harbor mutations in DDR genes or that acquire resistance to treatments.

Here, to search for factors that contribute to DNA repair in TNBC cells, we analyzed three genome-wide screenings for genes involved in the maintenance of genome integrity.[9–11] Intersection of the results uncovered the U2 small nuclear ribonucleoprotein particle (snRNP) complex as potential key factor for efficient DNA repair. The U2 snRNP is a component of the spliceosome, the machinery that catalyzes splicing of introns from precursor messenger RNAs (pre-mRNAs).[12] It is noteworthy that splicing is emerging as a biological process that is altered in human cancers,[13–15] including TNBC.[16–19] Moreover, mutations in the U2 snRNP protein SF3B1 enhance the response to PARPis in other tumors.[20] We found that transient splicing inhibition induced persistent DNA damage in TNBC cells, regardless of their HR status. Treatment of HRP TNBC cells with the SF3B1 inhibitor pladienolide B (PdB) hampered transcription and/or splicing of DDR genes, leading to a prolonged repression of DDR protein expression. Importantly, a pulse of PdB was sufficient to generate extended vulnerability to platinum-based agents and PARPi in HRP TNBC cells and patient-derived organoids (PDOs). These findings identify the U2 snRNP complex as an actionable target whose inhibition improves chemotherapy efficacy in HRP TNBCs.

RESULTS

Splicing inhibition induces DNA damage in TNBC cells regardless of their HR proficiency

GI is associated with tumor progression and metastasis in BC,[21] and its induction is exploited to improve the sensitivity to chemotherapy.[21,22] For instance, BRCA1/2-deficient BCs display higher GI levels and stronger response to PARPi and platinum-based drugs.[22] TNBCs have been reported to have higher levels of endogenous DNA damage than other BCs.[23–25] Moreover, the basal-like TNBC subtype has higher expression of DDR genes, which correlates with higher sensitivity to cisplatin.[26] However, whether GI is significantly higher in TNBCs was not directly investigated. The fraction of altered genome between samples in The Cancer Genome Atlas (TCGA) showed a higher GI in TNBCs with respect to other BCs (Figure 1A). Likewise, the chromosome instability index (CIN) was higher in TNBCs than in other BC samples from the Clinical Proteomic Tumor Analysis Consortium (CPTAC) (Figure 1A). These analyses are in line with the observation that TNBCs are highly susceptible to treatments that impact DNA integrity.[3]

To identify core regulators of genomic integrity, we queried three datasets generated by genome-wide small interfering RNA (siRNA) screenings for factors required for the phosphorylation of the histone variant H2AX (γH2AX),[9] an early marker of DNA damage, or HR efficiency.[10,11] Intersection between these datasets identified 96 common genes (Figure 1B; Table S1). Cellular component analysis of these genes highlighted an enrichment in proteins of the U2 snRNP complex (Figure 1C), one of the core particles of the spliceosome. The U2 snRNP recognizes the 3′ splice site (SS) at the end of introns, a step required at the early phase of the splicing reaction.[12,27] Notably, several drugs that directly or indirectly inhibit the U2 snRNP function are being explored in clinical trials as anti-cancer agents.[14,15,28] To test the impact of U2 snRNP inhibition on DNA integrity and cell viability, we employed three drugs with different chemical structure: PdB and thailanstatin A (ThailA), which target the U2 snRNP core protein SF3B1,[29–31] and indisulam, which targets the U2-associated factor of 65 kDA (U2AF65)-like protein RBM39.[32] Dose-response curves showed a similar impact of the three drugs on viability of basal-like (HCC1806) and mesenchymal-like (MDA-MB-231 and MDA-MB-436) TNBC cells (Figure 1D). HCC1806 cells were slightly more sensitive to indisulam (Figures 1D and 1E), likely because RBM39 depletion was faster than in mesenchymal-like TNBC cells (Figure S1A). Importantly, these TNBC cell lines display different sensitivity to clinically approved DNA-damaging agents. MDA-MB-436 cells harbor an inactivating mutation in *BRCA1*[26,33] and display hypersensitivity to PARPi (talazoparib and olaparib) and cisplatin (Figures 1E and S1B). By contrast, MDA-MB-231 are *BRCA1* wild type and more resistant to these clinically approved DNA-damaging drugs (Figure S1B), with a 50% inhibitory concentration (IC_{50}) ∼100-fold higher than that of MDA-MB-436 cells (Figure 1E). In line with the higher sensitivity to DNA damage of basal-like TNBCs,[26] the *BRCA1* wild-type HCC1806 cell line showed an intermediate sensitivity to these drugs (Figures 1E and S1B).

To test whether U2 snRNP inhibitors affect DNA damage in TNBC cells, we quantified the γH2AX foci by immunofluorescence analyses of mesenchymal TNBC cells exhibiting weaker (MDA-MB-436) or stronger (MDA-MB-231) HR proficiency. To avoid induction of apoptosis (Figure S1C), cells were treated for 24 h with a dose of PdB and ThailA, corresponding to the IC_{50} value, or with 3.3 μM indisulam. Since different DNA repair pathways are activated in a cell-cycle-dependent manner,[34] γH2AX foci were quantified in both cyclin A2-positive ($CCNA^+$; S/G2 phases) and negative ($CCNA^-$; G1 phase) cells. All splicing inhibitors significantly induced accumulation of γH2AX foci in $CCNA^+$ cells (Figures 1F and 1G), whereas the effect was much weaker in $CCNA^-$ cells (Figure S1D). Together, these findings suggest that pharmacological inhibition of U2 snRNP function, unlike canonical chemotherapeutic drugs, induces DNA damage in TNBC cells regardless of their BRCA status and HR proficiency.

Transient splicing inhibition persistently impairs the DDR in TNBC cells

Since splicing is an essential process, and its persistent inhibition is likely detrimental for all cells, we asked whether a transient treatment with splicing inhibitors was sufficient to exert long-lasting effects on DNA damage and cell survival. First, we tested whether splicing efficiency was recovered after transient spliceosome inhibition. Analyses of intron retention (IR) events in *RIOCK3* and *DNAJB1*, which have been shown previously to be sensitive to PdB treatment,[29] indicated that exposure to PdB for 6–16 h strongly impaired splicing efficiency. However, intron splicing was almost completely rescued after 24 h from drug removal in all cell lines (Figures 2A, 2B, and S2A). Moreover, nuclear fractionation assays followed by real-time qPCR analysis of chromatin-bound small nuclear RNAs (snRNAs) indicated that

CellPress
OPEN ACCESS

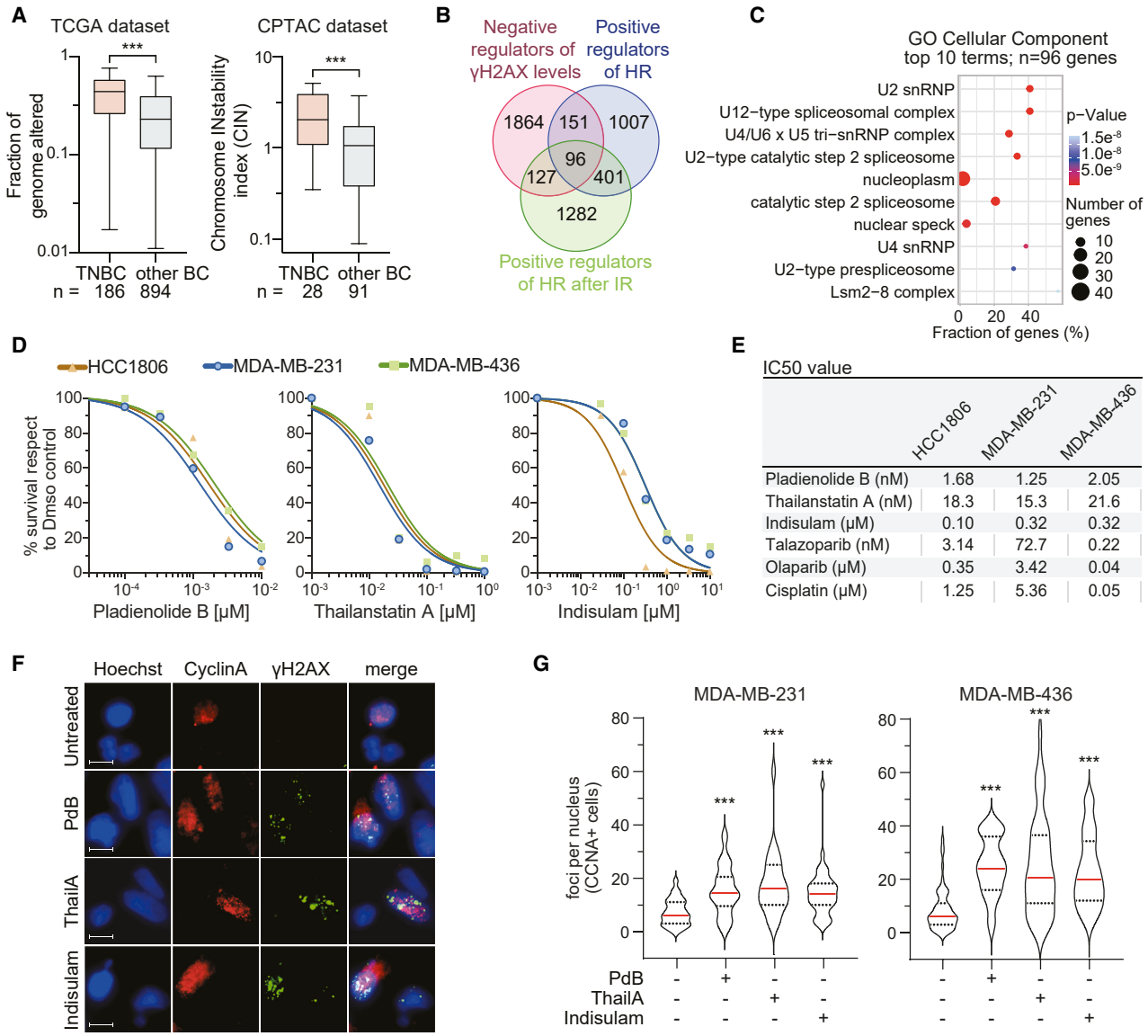

Figure 1. Splicing inhibition induces DNA damage and impairs viability in HRP TNBC

(A) Fraction of genomes altered and CIN in TNBC and other BC samples from TCGA (left) and CPTAC (right). The median, 5th/95th percentiles (whiskers), and number of samples are shown (unpaired Student's t test, ***$p < 0.001$).

(B) Overlap of regulators of genomic integrity retrieved from three siRNA screenings.

(C) GO term enrichment among the 96 common genes (modified Fisher's exact test).

(D) Crystal violet viability assays of TNBC cells exposed to splicing inhibitors for 6 days (mean of ≥3 experiments).

(E) Half-maximal inhibitory concentration (IC_{50}) values of the indicated drugs for each cell line, determined from fitting curves.

(F) Representative immunofluorescence images for γH2AX, Cyclin A, and Hoechst in MDA-MB-231 cells treated or not with splicing inhibitors for 24 h. Scale bar, 5 μm.

(G) Immunofluorescence quantification of γH2AX foci in $CCNA^+$ nuclei of MDA-MB-231 and MDA-MB-436 cells treated as indicated in (F). Violin plots show the median (red line) and interquartile range (black dotted line) of γH2AX foci in at least 100 nuclei of 2 independent experiments (two-tailed unpaired Student's t test with respect to DMSO, ***$p < 0.001$).

See also Figure S1 and Table S1.

short-term treatments with PdB resulted in selective depletion of U2 snRNA from chromatin (Figures 2C and S2C), without affecting overall U1 and U2 snRNA levels (Figure S2B). In line with reversibility of IR, U2 snRNA was also efficiently recovered onto chromatin upon drug removal (Figures 2C and S2C).

Next, we tested the impact of a PdB pulse on DNA damage in MDA-MB-231 cells, which are more resistant to DNA-damaging agents (Figures 1E and S1B). Accumulation of γH2AX foci was increased upon release from drug treatment in $CCNA^+$ (Figures 2D and S2D) and, to a lesser extent, $CCNA^-$ cells

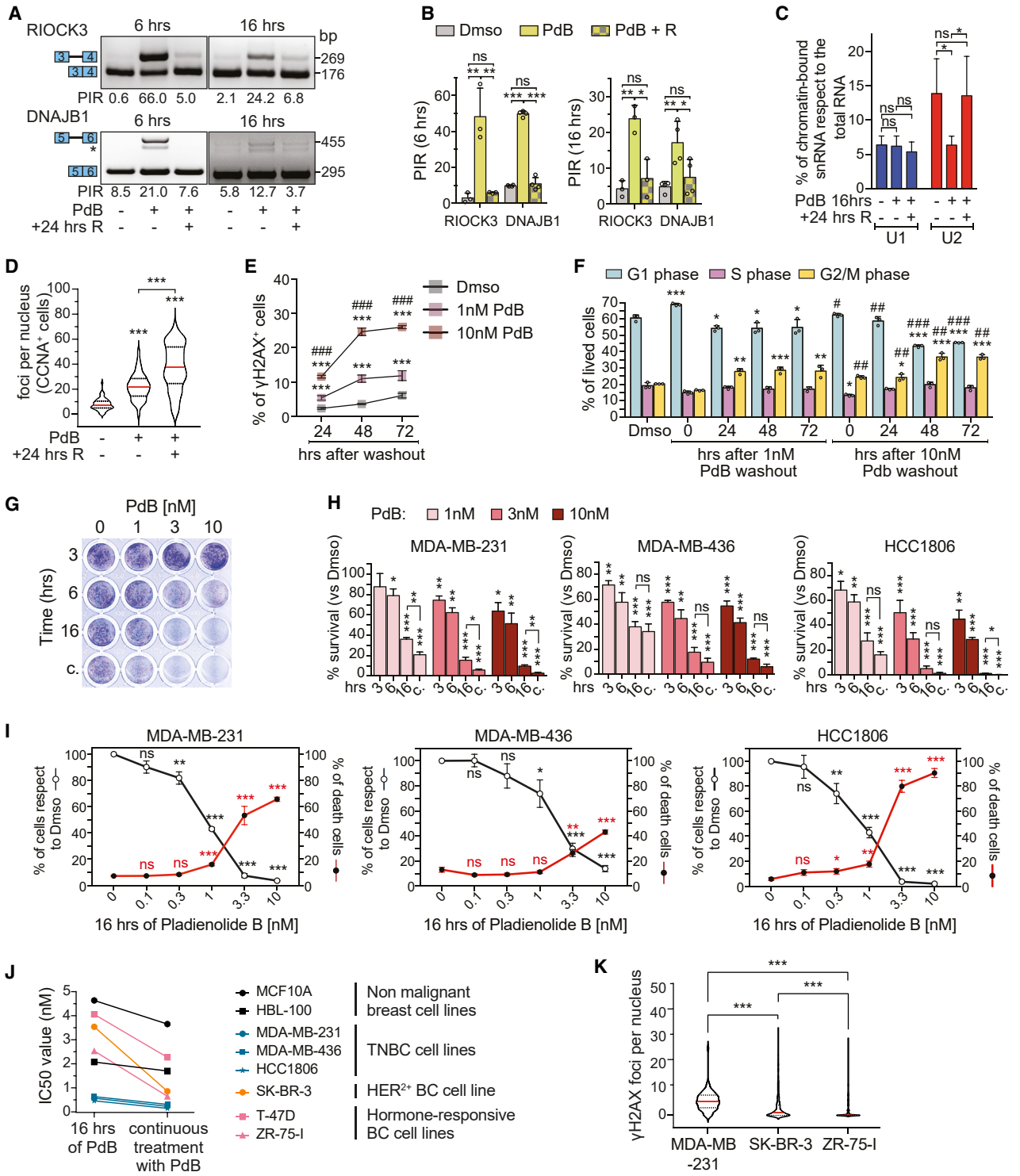

Figure 2. Transient splicing inhibition persistently impairs the DDR in TNBC cells

(A) RT-PCR analysis of the *RIOCK3* and *DNAJB1* IR events in MDA-MB-231 cells treated with 10 nM PdB with (R) or without 24-h recovery. *, non-specific band.

(B) Densitometric analysis of the percentage of IR (PIR) (mean ± SD, *n* = 3; unpaired Student's t test).

(C) Chromatin-associated snRNAs assayed by qPCR and calculated as percentage of input snRNA (mean ± SD, *n* = 3; paired Student's t test).

(D) Violin plots with median (red line) and interquartile range (black dotted line) of γH2AX foci in CCNA+ nuclei treated with 10 nM PdB for 16 h with (R) or without recovery. At least 100 nuclei of 2 experiments were evaluated (unpaired Student's t test).

(legend continued on next page)

(Figure S2E). Interestingly, accumulation of DNA damage during splicing recovery was not observed in non-TNBC cell lines, such as ER^+ (ZR-75-I) or $HER2^+$ (SK-BR-3) cells (Figures S2D, S2F, and S2G). Cytofluorimetric analysis of γH2AX-positive MDA-MB-231 cells confirmed that treatment with a 16-h pulse of sub-optimal (1 nM) or optimal (10 nM) concentration of PdB persistently impaired the repair of double-strand breaks (DSBs). Damaged cells increased over time after drug release (Figures 2E and S2H), and this effect was most prominent in S phase cells (Figure S2I). The PdB pulse also caused a dose-dependent accumulation of cells in G2 phase 24 h after drug removal, an effect that persisted (1 nM) or even increased (10 nM) after 48–72 h (Figure 2F). Thus, transient splicing inhibition elicits a long-lasting effect on DNA damage in HRP TNBC cells, which extends beyond its direct impact on splicing.

To evaluate whether transient splicing inhibition was sufficient to impair cell viability, we pulsed TNBC cells for 3–16 h with increasing concentrations of PdB, followed by 96-h release. The PdB pulse reduced cell number in a time- and dose-dependent manner in all cell lines (Figures 2G and 2H). At all doses tested, the 16-h pulse caused a similar growth inhibition as that obtained with continuous exposure to PdB (Figure 2H) or ThailA (Figure S3A). To evaluate whether growth inhibition was due to cell death or proliferation arrest, we pulsed cells for 16 h with increasing doses of splicing inhibitors and monitored them in real time for the following 96 h. Induction of cell death was achieved with higher doses of these drugs (3.3–10 nM PdB, 0.33-1μM ThailA), and this was associated with an almost complete arrest of cell growth (Figures 2I and S3B–S3D). Interestingly, cell death was more pronounced in *BRCA1* wild-type cells (HCC1806 and MDA-MB-231) than in the *BRCA1* mutated MDA-MB-436 cells (Figures 2I and S3C). By contrast, non-cancerous breast cells (MCF10A and HBL-100), ER^+ (T-47D, ZR-75-I), and $HER2^+$ (SK-BR-3) BC cells were more resistant to the PdB pulse, with IC_{50} values 3- to 9-fold higher than those of TNBC cell lines (Figures 2J, S3E, and S3F). Moreover, the two BC cell lines that are more sensitive to continuous treatment with PdB (SK-BR-3 and ZR-75-I) displayed an ∼4-fold increase in IC_{50} when PdB was administered as a 16-h pulse (Figures 2J, S3E, and S3F). The specific sensitivity of TNBC cells to the PdB pulse may depend on their intrinsic GI (Figure 1A), as also indicated by the higher levels of basal DNA damage in these cells with respect to other BC cells (Figure 2K) and the lack of persistent DNA damage accumulation in the latter (Figures S2F and S2G). These findings suggest that transient splicing inhibition triggers persistent DNA damage in GI-prone TNBC cells, regardless of their HR proficiency, resulting in perturbation of cell cycle progression, inhibition of proliferation, and induction of cell death.

Splicing inhibition globally alters transcription and splicing of DDR genes

To further investigate the impact of splicing inhibition on the DDR, we profiled the transcriptome of TNBC cells acutely treated (6 h) with PdB. Splicing inhibition pervasively altered the MDA-MB-231 transcriptome, with 47.4% of the expressed genes being modulated at the gene expression (GE) level and 30.7% at the splicing level (Figure S4A; Tables S2 and S3). We found a significant overlap between GE- and splicing-regulated genes (Figure S4B). While most GE-regulated genes were repressed, a large fraction (43.1%) was also up-regulated (Figure S4C), indicating that cells react to splicing inhibition by activating GE programs. At the splicing level, exon cassette (EC) was the most regulated pattern, and PdB mostly repressed the inclusion of these exons (Figures S4D and S4E). However, many splicing events (56.1%) were not annotated as alternative events in the reference FAST database.[35] Most of these unannotated events (95%) are IR events (Figures S4E and S4F), documenting a widespread inhibition of constitutive splicing reactions.

Gene Ontology (GO) analysis of genes downregulated by PdB treatment indicated that terms related to replication fork processing and DNA repair were significantly enriched (Figure S4G). Strikingly, 68.8% of the genes included in the GO term "response to DNA damage" (Table S4) were modulated at the GE and/or splicing level (Figure 3A), suggesting that DDR genes are particularly affected by PdB treatment. We also observed that DDR genes are expressed at a significantly higher level than all other genes in MDA-MB-231 cells (Figure S4H). Furthermore, they feature a larger number of smaller exons but not increased intron or overall length (Figures S4H). Increased exon number was also observed among the regulated DDR genes with respect to other regulated genes (Figure 3B). Moreover, we observed a larger and more significant overlap between GE- and splicing-regulated DDR genes (Figure 3C) with respect to all genes (Figure S4B). DDR genes were also more downregulated than other genes (Figure 3D), while at the splicing level, there was a higher proportion of up-regulated IR and downregulated EC events with respect to all other regulated genes (Figure 3E). We reasoned that the larger number of exon-intron junctions in DDR genes may lead to their unproductive processing during transcription, thus impacting on their expression. Indeed, meta-analysis of read coverage revealed that downregulated and splicing-regulated DDR genes displayed a progressive reduction of reads toward the 3′-end of the transcription unit in PdB-treated cells (Figures 3F and 3G). This feature was much less pronounced in the other regulated genes (Figure S4I), suggesting that the increased number of exons imposes on DDR genes a dependency on highly efficient splicing.

(E) Flow cytometry analysis of γH2AX-positive cells after PdB removal (mean ± SD, $n = 3$, unpaired Student's t test with respect to DMSO [*] or 1 nM PdB [#]).
(F) Cell cycle flow cytometry analysis of MDA-MB-231 cells treated for 16 h with DMSO or PdB (time 0), followed by the indicated time after drug release (mean ± SD, $n = 3$, unpaired Student's t test with respect to DMSO [*] or 1 nM PdB [#]).
(G and H) Representative (G) and quantitative (H) crystal violet assays of TNBC cells treated with a 3-, 6- or 16-h pulse or continuously (c.; 96 h) with increasing PdB concentrations (% DMSO treatment, mean ± SEM, $n \geq 3$, unpaired Student's t test).
(I) Total cell (black) and dying cells (red) cultured for 96 h after the PdB pulse at the indicated concentrations (means ± SEM, $n \geq 5$).
(J) IC_{50} values of PdB were determined after 96 h of pulse or continuous treatment using fitting curves.
(K) Violin plots showing the median (red line) and interquartile range (black dotted line) of γH2AX counts per nucleus in at least 200 nuclei from 2 experiments (two-tailed unpaired Student's t test, $^{***}p < 0.001$).
See also Figures S2 and S3.

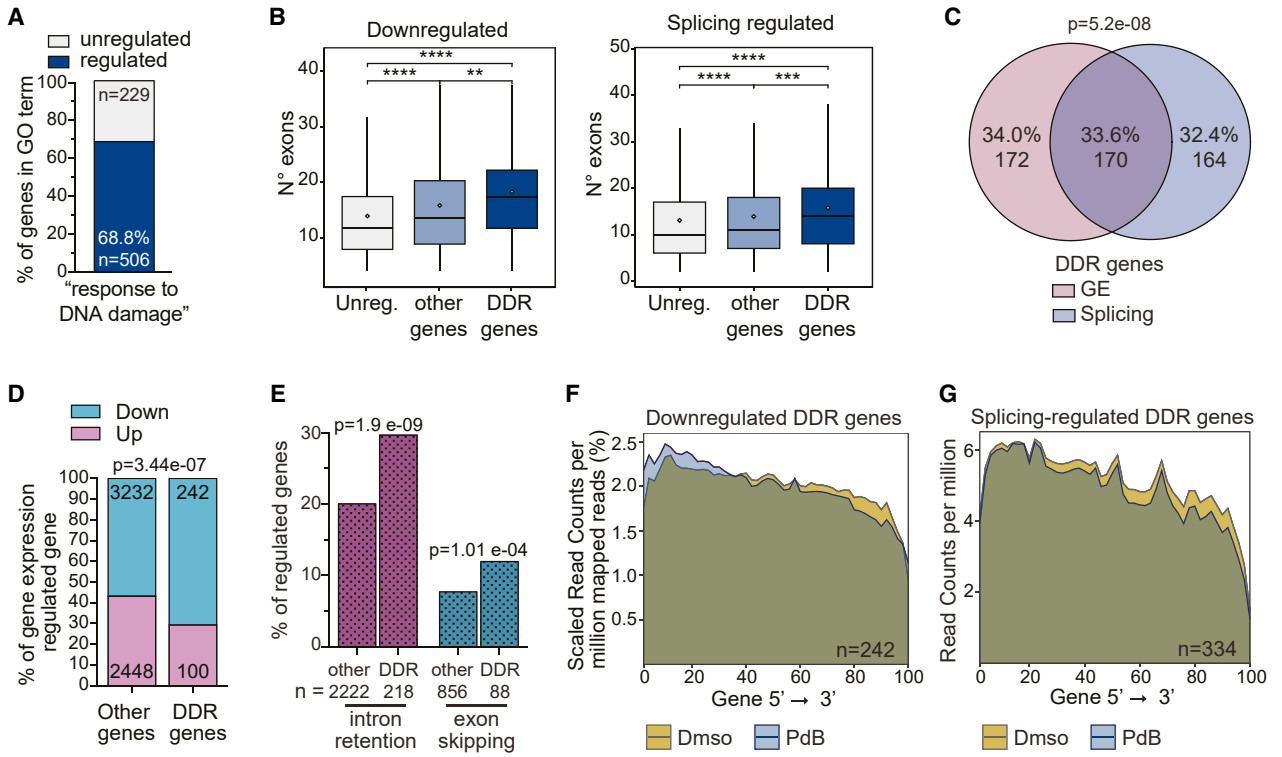

Figure 3. PdB impairs RNA processing regulation of DDR genes in TNBC cells

(A) Percentage and number of DDR genes regulated by PdB (blue bar).

(B) Number of exons in unregulated (gray), other regulated (light blue), and DDR-regulated (dark blue) genes that undergo downregulation (left) or splicing regulation (right) by PdB.

(C) Overlap between GE- and splicing-regulated DDR genes (hypergeometric test).

(D) Percentage and number of upregulated (magenta) and downregulated (cyan) transcripts by PdB belonging to DDR genes or other genes (Fisher's exact test).

(E) Percentage and number of DDR or other genes that undergo IR or EC events in PdB-treated cells (Fisher's exact test).

(F and G) Metagene plots showing the percentage of read counts per million mapped reads distribution within the body of downregulated (F) and splicing-regulated DDR genes (G) in DMSO-treated (yellow) or PdB-treated (blue) cells.

See also Figure S4, Tables S2–S4.

DDR proteins are persistently repressed upon transient splicing inhibition

Dissection of the regulated DDR genes for their involvement in biological processes indicated that the "DNA repair" class was the most impacted at the splicing level (57% of the genes) (Figure 4A). Moreover, most GE-regulated genes in this class were repressed (76%, *n* = 177). In contrast, genes of the "apoptotic signal" class were equally up- and downregulated (Figure 4A). All the pathways involved in DNA repair were strongly affected at the GE or splicing level by PdB (Figure 4A), suggesting that U2 snRNP inhibition impairs HR as well as other mechanisms of DNA repair. PdB regulates genes encoding factors that are essential for genome integrity. For instance, the BRCA1, BRCA2, ATRIP, and RAD51 proteins ensure the precise repair of DNA lesions by HR, and their transcript levels were decreased by the treatment (Table S2). Analysis by qPCR confirmed the decreased expression of BRCA1, BRCA2, ATRIP, and RAD51 transcripts by PdB, ThailA, and indisulam (Figures 4B–4D). Among the DDR genes regulated at the splicing level, we noted *RNF8*, which encodes an E3-ubiquitin ligase that stabilizes γH2AX and ensures the recruitment of other DDR proteins at the site of the lesion.[36] Splicing inhibitors promoted the usage of an alternative 3′ SS(a3′SS) in *RNF8* intron 2, introducing 106 additional nucleotides into exon 3 and disrupting the protein open reading frame (Figure 4E). Coherently, all these DDR proteins were strongly reduced upon treatment with U2 snRNP inhibitors (Figures S4J and S4K).

Many DDR genes regulated at the GE level also showed defects in intron splicing. As exemplified by the *BRCA2* and *ATRIP* genes, PdB induced retention of intron 1, an event that was associated with progressive reduction of read coverage in distal exons (Figures 4F and 4G). Likewise, selection of the a3′SS in *RNF8* was associated with a general increase in intron reads and a sharp reduction of read coverage in downstream constitutive exons (Figure 4H), which was confirmed by qPCR analysis (exon 3-exon 5; Figure S4L). Together with the metagene analyses, these findings suggest that high fidelity of RNA processing is required for the proper expression of DDR transcripts in TNBC cells.

Since the PdB pulse inhibited the splicing process only transiently, while it caused persistent DNA damage (Figure 2), we

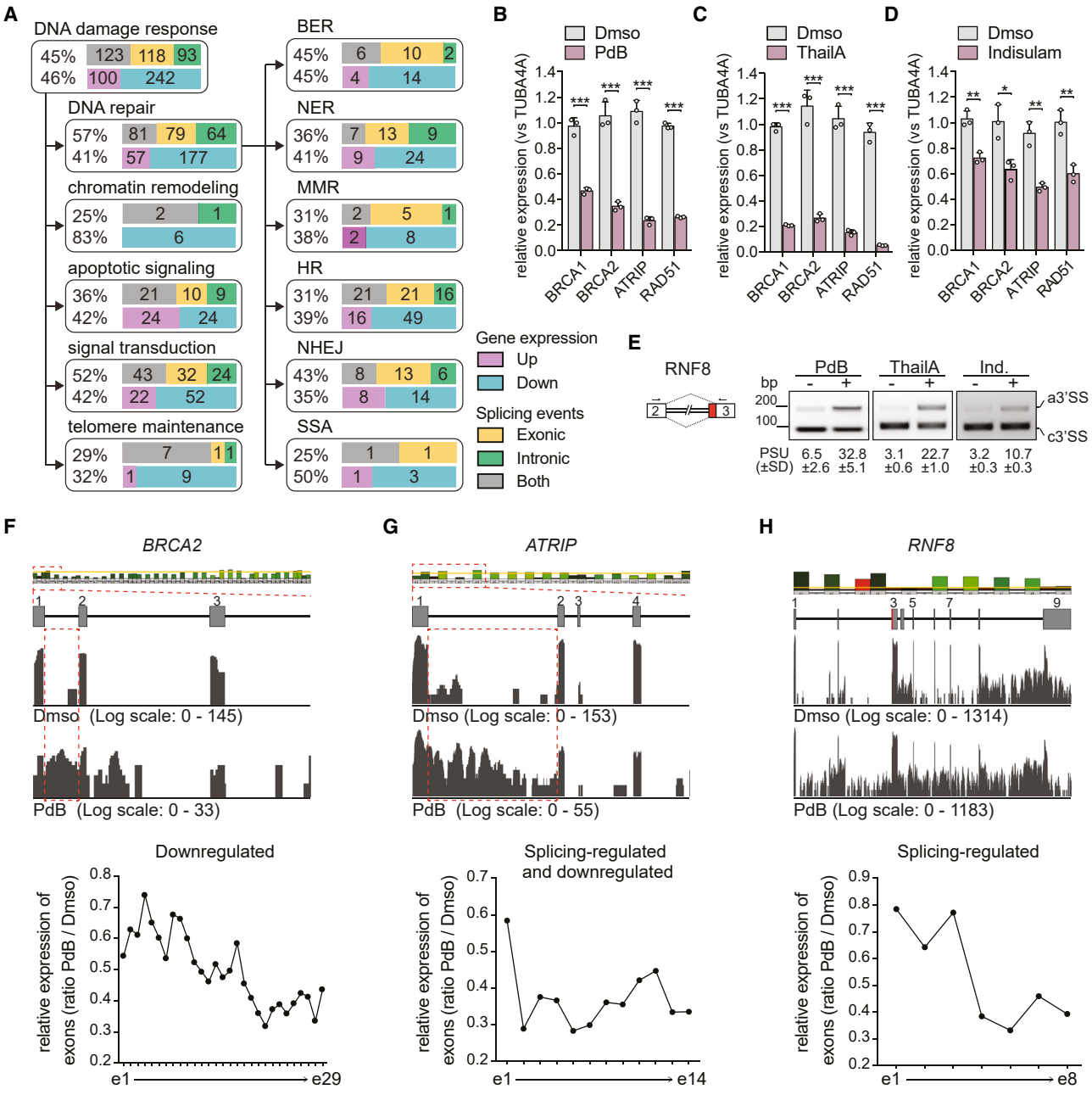

Figure 4. Splicing inhibition downregulates the expression of DDR genes

(A) Hierarchical representation of DDR-related biological processes. Percentages of genes regulated by splicing or GE are reported for each term. Bars show the number of downregulated (cyan) and upregulated (magenta) genes and the number of genes regulated by intronic (jade green), exonic (yellow), or both (gray) splicing events.

(B–D) qPCR analyses of DDR genes (fold change with respect to DMSO) in MDA-MB-231 cells treated with 10 nM PdB for 6 h (B), 1 μM ThailA for 16 h (C), and 3.3 μM indisulam for 24 h (D) (mean ± SD, $n = 3$, unpaired Student's t test).

(E) RT-PCR analyses for the a3′SS in RNF8 (left). Densitometric analysis of the percentage of alternative SS usage (PSU) is shown (mean ± SD, $n = 3$).

(F–H) RNA-seq reads profiles of DDR genes in cells treated with DMSO (top) or PdB (bottom). Sequence reads (vertical gray lines), exons (gray boxes), introns (horizontal lines), and the alternative exon generated by 3′SS usage in RNF8 (red box) are shown. Line charts below show the expression levels of *BRCA2* (F), *ATRIP* (G) and *RNF8* (H) constitutive exons in PdB-treated cells.

See also Figure S4.

asked whether expression of DDR transcripts was also permanently impaired. RNA sequencing (RNA-seq) analysis confirmed that almost all DDR transcripts (91.8%) were also affected by 16-h treatment with PdB (Figure S5A). However, expression of most DDR downregulated genes (63%), splicing defects (75%), and unproductive processing of DDR transcripts were rescued upon recovery from the PdB pulse (Figures S5B and S5C). Coherently, qPCR analysis of the 3′ end region of DDR transcripts indicated that their levels were fully rescued after PdB removal (Figure 5A). For splicing evaluation, we tested the retention of the first intron, because recent findings indicated that PdB impaired its processing more strongly than downstream introns.[37,38] PdB treatment caused IR in all the DDR genes tested, with a strong effect (>10- to 100-fold) observed particularly in the *BRCA2*, *ATRIP*, and *RAD51* genes. Splicing of these introns was completely (*ATRIP* and *RAD51*) or almost completely (*BRCA2*) rescued in the next 24 h, except for *BRCA1* intron 1 (Figure 5B). Likewise, aberrant selection of the RNF8 a3′SS was partially recovered (>50%) at this time point, together with the rescue of its expression (Figure S5D). Splicing recovery was also observed by comparing the ratio of proximal versus distal intron expression, which was increased by PdB in all DDR genes, except for *BRCA1*, and returned to basal levels after drug release (Figure S5E). Surprisingly, however, DDR protein expression was not rescued. Except for RNF8, whose level paralleled the splicing regulation, DDR proteins remained at low levels upon drug removal (Figures 5C and S5F). Notably, the BRCA1 and BRCA2 proteins were almost completely depleted by treatment with PdB and subsequent release (Figure 5C), thus mimicking a sustained BRCAness condition. Moreover, the ATRIP protein was significantly reduced after drug removal (Figure 5C). Repression of protein expression by PdB was not a general feature, as proteins encoded by other transcripts downregulated at similar levels (DDX21, FIP1L1, CDK7) underwent only a mild reduction during the pulse, and their expression was almost completely rescued after drug removal (Figures 5C and S5F). Moreover, except for RAD51, lower DDR protein levels persisted up to 48 h after PdB removal, and this effect was associated with increased DNA damage, as indicated by the phosphorylation of H2AX and CHEK1 (Figure S5G).

BRCA1 protein levels oscillate during the cell cycle.[39] Since PdB caused accumulation of cells in the G2/M phase of the cycle, we asked whether this effect was correlated with reduced DDR protein expression. Synchronization of MDA-MB-231 cells in late G1 with mimosine and subsequent release showed rather stable levels of DDR proteins, with a weak increase of BRCA2 observed upon drug release and a significant reduction of BRCA1 only in cells under mimosine block (Figures S5H and S5I). Next, we sorted cells according to their DNA content and analyzed the expression of BRCA1/2 proteins under different treatment conditions (Figure S5J). The PdB pulse impaired the expression of BRCA1/2 proteins regardless of the cell cycle phase, and this effect was maintained after drug release (Figure S5J). Thus, the persistent effect of PdB on DDR proteins is unrelated to its effects on the cell cycle.

To assess whether uncoupling between transcription and protein expression was caused by a general latency in accumulation of DDR proteins, we exposed MDA-MB-231 cells to a reversible transcriptional inhibition by treatment with 5,6-dichloro-1-beta-D-ribofuranosylbenzimidazole. Upon 24-h recovery from transcription inhibition, DDR transcripts and proteins were fully recovered (Figures S5K and S5L). DDR proteins are also extensively modulated by ubiquitination-dependent protein degradation.[40] However, while the proteasome inhibitor MG132 induced the accumulation of BRCA1, BRCA2, RAD51, and RNF8 proteins in control cells, it did not affect their expression in PdB-treated cells or upon their recovery from splicing inhibition (Figure S5M). Thus, persistent repression of DDR protein expression is specifically associated with a transient inhibition of splicing.

Since DDR pre-mRNAs are characterized by higher numbers of exon-intron junctions (Figure S4H), we hypothesized that they might recover more slowly from splicing inhibition because they would more likely retain incompletely spliced introns and/or aberrantly spliced exons. To test this hypothesis, we focused on BRCA1, BRCA2, and ATRIP, which showed the strongest and more persistent uncoupling between transcription and protein accumulation (Figures 5A and 5C). Transcripts from the *BRCA1/2* and, to a lesser extent, *ATRIP* genes were inefficiently exported to the cytoplasm with respect to housekeeping genes (*TUBA4A* and *ACTN1*) in untreated cells (Figure 5D). Furthermore, the cytoplasmic pool of BRCA1/2 mRNAs was reduced by the PdB pulse (Figures 5E and S5N). ATRIP transcripts also accumulated in the cytoplasm, albeit to a lesser extent than in the nucleus, indicating slow processing or export efficiency for these transcripts also. Polysome profiling indicated that cells are actively translating 24 h after PdB removal (Figure 5F), as also indicated by the efficient loading of the actin mRNA onto the polysome fractions (Figure 5G). However, polysome loading of the BRCA2 and ATRIP mRNA was reduced significantly (>2-fold; Figure 5G). Together, these data indicate that inefficient nuclear export (BRCA1 and BRCA2) and translation (BRCA2 and ATRIP) of DDR transcripts account for the lack of protein expression rescue after a pulse of splicing inhibition.

Transient splicing inhibition causes persistent repression of DNA repair in TNBC PDOs

To validate these findings in TNBC models that are representative of actual disease, we developed three PDO lines from tumors that were wild type for both *BRCA1* and *BRCA2* (Figures S6A; Table S5). PDO-39 was derived from the diagnostic biopsy of a patient who underwent pathological complete response (pCR) to subsequent neoadjuvant chemotherapy, whereas PDO-21 and PDO-46 were obtained from tumors that were refractory to cytotoxic chemotherapy (Table S5). Regardless of the sensitivity of the original tumor to chemotherapy, all PDOs were sensitive to both continuous and transient treatment with PdB, similar to what was observed with TNBC cell lines (Figures S6B and S6C). At suboptimal doses (3 nM), the PdB pulse was sufficient to reduce the number and size of all PDO lines (Figures 6A–6C), albeit with variable efficacy. The PdB pulse exerted a transient effect on transcription and splicing of the first intron in DDR genes (Figure 6D and S6D) as well as on splicing of the a3′SS in RNF8 (Figure S6E). However, DDR proteins were persistently repressed, with the largest recovery (60% of untreated) being observed for RNF8 (Figures 6E and

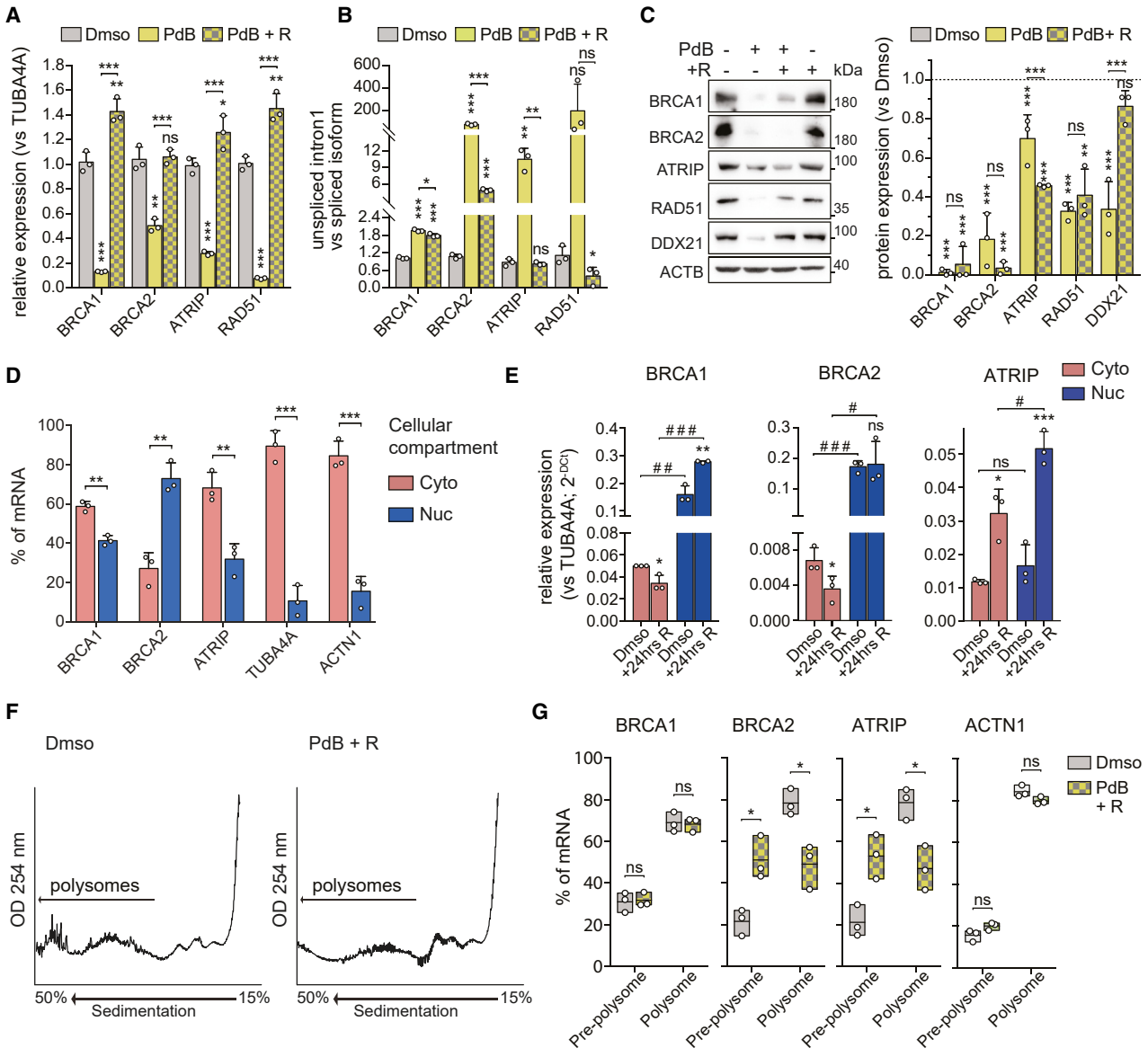

Figure 5. Transient splicing inhibition persistently alters expression of DDR proteins

(A and B) qPCR analyses of the expression (A) and unspliced/spliced first intron ratio (B) of DDR genes in cells treated with PdB for 16 h with (+R) or without 24-h recovery (fold change relative to DMSO, mean ± SD, *n* = 3, unpaired Student's t test).

(C) Western blot analysis of DDX21 and DDR proteins (left). Densitometric analyses were done using ACTB as a control (right) (mean ± SD, *n* = 3, unpaired Student's t test).

(D) qPCR analyses of DDR transcripts in MDA-MB-231 nuclei and cytoplasm. TUBA4A and ACTN1 were used as controls (means ± SD, *n* = 3, unpaired Student's t test).

(E) qPCR analyses of DDR transcripts in nuclei and cytoplasm after 24 h of PdB washout (+R) or in control conditions (DMSO) (means ± SD, *n* = 3, unpaired Student's t test with respect to DMSO [*] or between cellular compartments of the same samples [#]).

(F) Polysome profiles of cells cultured in control conditions (left) or for 24 h after PdB pulse (right). Polysome-containing fractions are indicated by an arrow.

(G) Floating bars (min-to-max) graphs showing the percentage of DDR transcripts associated with polysome and pre-polysome fractions calculated by qPCR. ACTN1 was used as a control (mean ± SD, *n* = 3, unpaired Student's t test).

See also Figure S5.

6F). The suboptimal PdB pulse was also sufficient to induce accumulation of γH2AX foci in the cells of all PDOs (Figures 6G, 6H, and S6F). These results indicate that the effect of transient U2 snRNP inhibition is highly reproducible in multiple TNBC models. Moreover, they show that a short pulse of PdB persistently represses the DNA repair machinery in HRP cells, including those resistant to conventional chemotherapy, thus possibly enhancing vulnerability to genotoxic drugs.

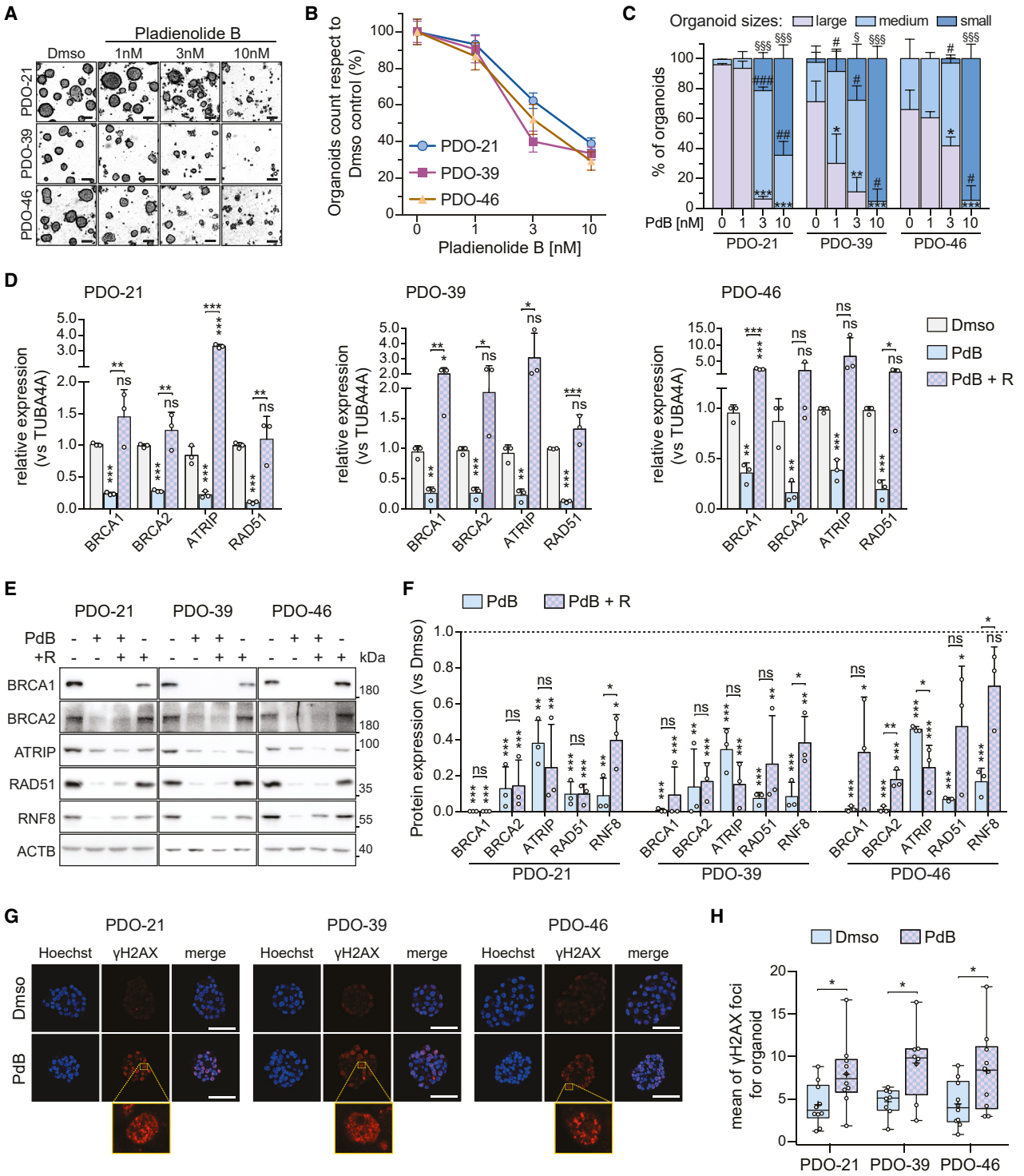

Figure 6. Transient splicing inhibition impairs the DDR and improves chemotherapy response in TNBC PDOs

(A) Bright-field images of PDO cultures treated with DMSO or PdB (scale bar, 100 μm).

(B) Organoid number in cultures treated for 24 h with PdB and counted 96 h after removal (%PDO number with respect to DMSO, mean ± SEM, $n = 9$).

(C) Percentage of large, medium, and small PDOs for conditions described in (B) (mean ± SD, $n = 3$, unpaired Student's t test for small [*], medium [#], and large [§] PDOs with respect to DMSO).

(D) qPCR analyses of DDR genes in cultures exposed to 10 nM PdB for 24 h with (+R) or without 24-h recovery (mean ± SD, $n = 3$, unpaired Student's t test).

(E) Western blot of DDR proteins in PDOs.

(legend continued on next page)

Splicing inhibition enhances vulnerability to DNA-damaging agents in HRP TNBC

Platinum compounds and PARPis have higher activity in *BRCA1/2*-mutated TNBCs.[41] Thus, we asked whether the PdB pulse enhances sensitivity to cisplatin or PARPis in HRP TNBC models. MDA-MB-231 cells were pretreated for 6 or 16 h with a suboptimal dose of PdB (3.3 and 1 nM, respectively) and either released in control medium or in the presence of suboptimal doses of cisplatin (3.3 μM) or talazoparib (33 nM) for 48 h. Phosphorylation of H2AX and cleavage of PARP1, another marker of genotoxic stress and apoptosis, indicated that transient U2 snRNP inhibition significantly increases DNA damage with respect to single chemotherapeutic treatments (Figures 7A and S7A). Sequential combined treatments also caused a larger increase in γH2AX-positive cells, which persisted for up to 72 h (Figures 7B and S7B). Cisplatin and talazoparib caused accumulation of cells in S/G2 phases at 24 h. However, a fraction of cells completed mitosis and re-entered the G1 phase within 72 h (Figures 7C, S7B, and S7C). Notably, at this later time point, the cells that re-entered G1 still displayed γH2AX staining (Figure S7B), indicative of persistent DNA damage that is transmitted to daughter cells. By contrast, pre-treatment with PdB delayed the progression of γH2AX-positive cells from S to G2 phase at 24–48 h (Figure 7C) and impeded completion of mitosis and re-entry into G1 phase at 72 h (Figures 7C, S7B, and S7C). This result is consistent with the inability of cells to withstand DNA damage after combined treatment. Accordingly, the sequential treatments completely halted cell growth and enhanced cell death with respect to cisplatin or talazoparib alone (Figures 7D, S7D, and S7E).

To further evaluate the interaction between splicing inhibition and chemotherapy, we performed pre-treatments with PdB for 6–16 h, followed by continuous treatment with increasing doses of cisplatin or talazoparib. By comparing MDA-MB-231 growth inhibition with respect to the single treatments, we observed a synergistic effect of the combined treatments (combination index < 1) for almost all doses and times tested (Figures 7E and S7F).

The addition of platinum agents (cisplatin or carboplatin) to neoadjuvant treatment is associated with significantly higher rates of pCR, especially in HRD tumors.[1] Furthermore, optimization of neoadjuvant treatments to increase the pCR rate is thought to be necessary to improve the prognosis and clinical course of HRP TNBC patients.[42] Thus, we employed PDO lines from patients who responded differently to neoadjuvant therapy to test the benefit of PdB pre-treatment in pre-clinical models of TNBC. PDO-39 viability was significantly impaired by 10 μM carboplatin, while that of neoadjuvant-resistant PDO-21 and PDO-46 was affected only at higher doses (Figure S7G). Moreover, a high dosage of carboplatin (33 μM) alone significantly increased DSB levels in PDO-39 and PDO-46 but not in PDO-21 (Figures 7F and 7G). Importantly, sequential combination of PdB and carboplatin exerted a synergic effect in all PDOs, regardless of the intrinsic sensitivity of the tumor to chemotherapy (Figures 7H, S7G, and S7H). This synergic effect was accompanied by enhanced induction of DNA damage in all PDO lines (Figure 7G). Collectively, these findings indicate that transient splicing inhibition persistently impairs the DDR and enhances the cytotoxic effects of DNA-damaging chemotherapy in HRP TNBC.

DISCUSSION

Management of TNBC patients includes neoadjuvant chemotherapy followed by surgical resection and adjuvant therapy.[3,43] However, while most TNBCs are sensitive to chemotherapy, a fraction of them relapse with time and progress to metastatic stages. Moreover, a minority of patients, enriched in HRP TNBC, do not respond efficiently to neoadjuvant chemotherapy. Thus, development of more efficacious treatments for TNBC that completely eradicate the tumor cells during chemotherapy is needed to improve the prognosis and clinical outcome of TNBC patients. Successful strategies may require the identification of predictive biomarkers for stratification of patients, beyond the HRD-associated mutations in DDR genes, and combined treatments that enhance chemotherapy efficacy.[21] This study shows that transient impairment of splicing is sufficient to induce persistent DNA damage by suppressing the expression of several DDR proteins. Moreover, this short-term treatment enhanced the effect of chemotherapy in multiple HRP TNBC models, including two organoid lines generated from tumors that were resistant to neoadjuvant chemotherapy. These findings suggest that transient splicing inhibition generates an actionable vulnerability in HRP TNBC, which may improve their response to current treatments.

A crucial crosstalk exists between RNA processing regulation, the DDR, and genome integrity.[44–46] Splicing factors, like RBMX[10] and EWS,[47] regulate select DDR genes, while DDR proteins, like BRCA1 and BCLAF1, associate with splicing factors in response to DNA damage and modulate splicing of genes involved in DNA repair.[48] Furthermore, cancer-associated mutations in splicing factors have been shown to induce DNA damage and GI in cancer cells.[20,49,50] Interestingly, a recent report documented that mutations causing an HRD phenotype in cancer are highly enriched in RNA binding proteins (RBP) genes and that these RBPs contribute to either the physical repair of the DNA damage or the expression of DDR genes.[51] Accordingly, our computational analyses of genes associated with the DDR or GI pointed to the strong enrichment of splicing factors, particularly of U2 snRNP components. Notably, U2 snRNP-related factors are frequently mutated in human cancers.[14,15] Here, we show that low doses of U2 snRNP-targeting drugs induce persistent DNA damage in TNBC cells regardless of their HR status.

(F) Densitometric analyses of western blots shown in (E) using ACTB as loading control (mean ± SD, $n = 3$, unpaired Student's t test).
(G) γH2AX and Hoechst immunofluorescence analysis of PDOs treated as indicated (48 h). Magnification insets show the γH2AX foci in the dashed boxed cells (scale bar, 40 μm).
(H) Boxplots showing median and interquartile range of average γH2AX foci counted for each PDO treated as in (G). Error bars represent min and max value. The + symbol indicates the mean value ($n \geq 8$, unpaired Student's t test).
See also Figure S6 and Table S5.

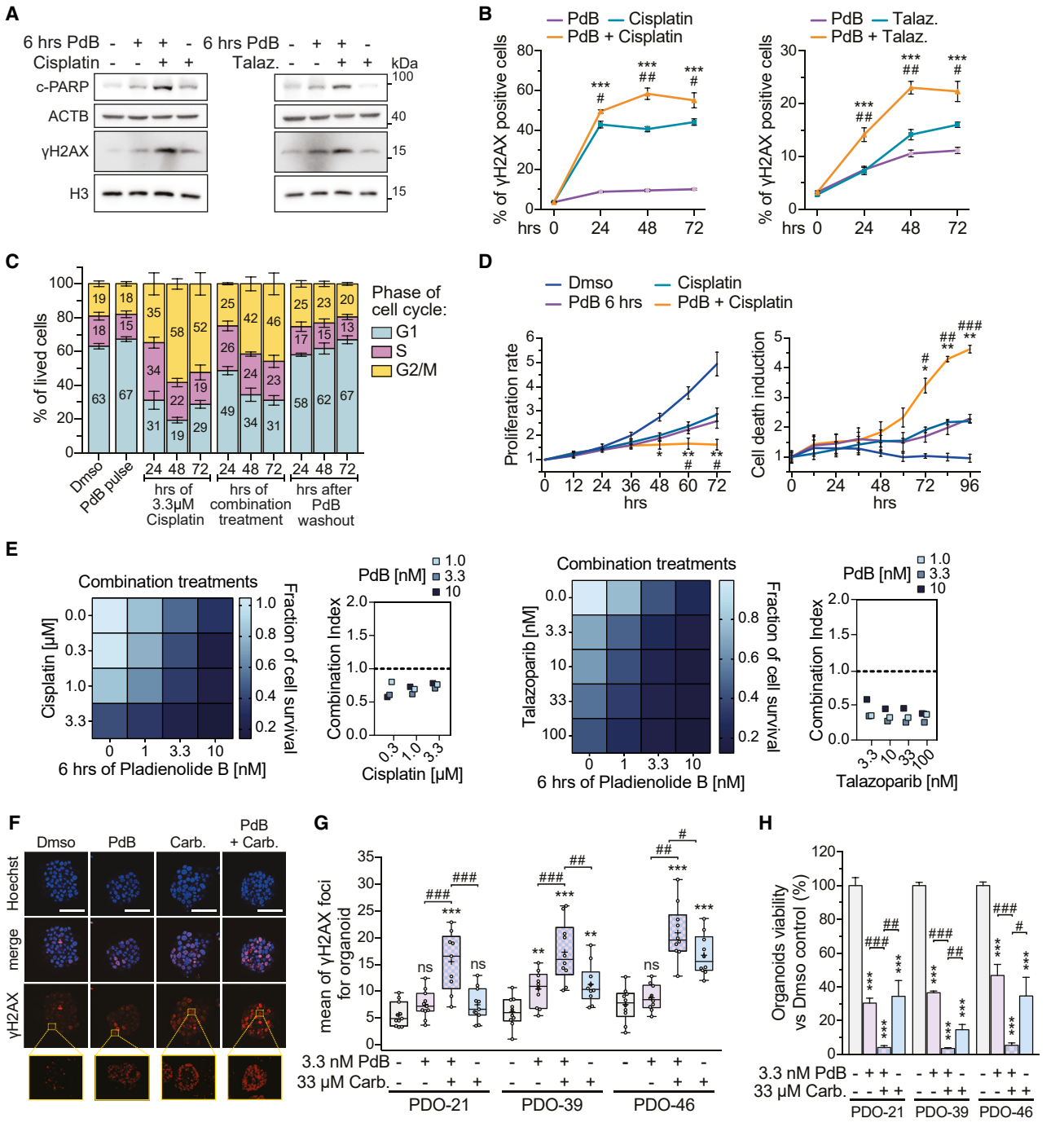

Figure 7. Transient splicing inhibition enhances chemotherapy efficacy in HRP TNBC cells and PDOs

(A) Western blot of cleaved PARP and γH2AX in MDA-MB-231 cells exposed to single or sequential treatments with 3.3 nM PdB for 6 h and 3.3 μM cisplatin or 33 nM talazoparib for 48 h.

(B) Flow cytometry analysis of γH2AX-positive cells pre-treated with 1 nM PdB for 16 h and released in control medium or in the presence of cisplatin (left) or talazoparib (right) (mean ± SD, *n* = 3, unpaired Student's t test with respect to PdB [*] or cisplatin/talazoparib [#]).

(C) Cell cycle distribution, determined by flow cytometry, of cells treated for 16 h with DMSO or 1 nM PdB, followed by an additional 24–72 h with vehicle or cisplatin (mean ± SD, *n* = 3).

(D) Proliferation rate (left) and induction of cell death (right) in the sequential treatments described in (A) (ratio between the number of stained cells at each time point with respect to time 0, means ± SEM, *n* = 3, unpaired Student's t test for each time point with respect to PdB-treated cells [*] or cisplatin-treated cells [#]).

(legend continued on next page)

Likewise, PDO lines derived from tumors displaying opposite responses to chemotherapy accumulated DNA damage upon transient treatment with PdB. This response is specific for GI-prone TNBC, as it was not observed in cells of other BCs, which were also less sensitive to PdB. Thus, transient splicing inhibition strongly impairs the DDR in TNBC cells, regardless of their sensitivity to chemotherapy.

PdB derivatives have shown promising activities in tumors harboring splicing factor mutations and are being tested in clinical trials.[14,15,52] Pre-clinical models of other cancer types, including cohesin-mutant leukemia and MYC-driven cancer, have also shown sensitivity to SF3B1 inhibition.[53–55] However, since splicing is an essential cellular process, lowering the concentration of these inhibitors is important to increase tolerability of treatments. Previous studies showed that cancer cells with high transcriptional rates, such as those harboring *MYC* amplification, are more vulnerable to splicing inhibition due to the increased burden imposed on the splicing machinery by the accumulation of pre-mRNAs.[53,54] Here, we found that DDR genes, whose structure is characterized by numerous small exons and that are expressed at high levels in TNBC, are particularly vulnerable to splicing inhibition. A brief PdB pulse impaired the expression of ~70% of the DDR genes in HRP TNBC cells. Thus, DDR genes comprising many exon-intron junctions are more likely to be affected by splicing inhibition because of the numerous splicing reactions required to process them. For instance, *BRCA1/2* and *ATRIP*, which all comprise >15 exons, were among the most affected genes. Our data also indicate that all pathways involved in the repair of DNA damage are repressed by splicing inhibition, which likely causes the irreparable defects and consequent cell death. The long-lasting effects of a transient PdB treatment on TNBC cell viability relies on the uncoupling between the recovery in DDR transcript and protein expression. Indeed, while the effects of the PdB pulse on transcription and splicing is mostly transient, several DDR proteins remain repressed for a prolonged time. We speculate that, due to the increased number of introns that characterize their genomic organization, these genes are more likely than others to retain introns in their pre-mRNAs during recovery from the stress of splicing inhibition. Notably, a large fraction of BRCA1 and BRCA2 polyadenylated transcripts is retained in the nucleus even in the absence of treatments, suggesting that they are still incompletely processed. In the case of ATRIP, while transcripts were exported in the cytoplasm during the recovery from PdB, they were translated inefficiently, likely due to aberrant processing. At the same time, recovery of transcript and protein expression of other non-DDR genes that are also transiently repressed by the PdB pulse, such as DDX21, occurred concomitantly. Mechanistically, our model differs from others that also report the susceptibility of DDR genes to transcription-associated RNA processing defects. For instance, DDR genes with long introns are particularly susceptible to inhibition of the transcriptional kinase CDK12, which reduces transcription elongation and triggers premature termination in introns.[56] However, PdB-regulated DDR genes are not characterized by increased intron length. Moreover, the persistent repression of DDR proteins after transient splicing inhibition is observed even when the 3′ end of their transcripts is produced. Together, these observations indicate that the high number of exon-intron junctions of DDR genes exposes them to a strong dependency on efficient splicing.

BRCA1 and BRCA2 assemble the repair machinery at the site of damage and promote HR-mediated repair.[6] ATRIP binds to single-strand DNA and interacts with the ATR kinase to resolve DNA replication fork stress,[57] a defect that is enhanced by SF3B1 mutations.[20,50] Thus, a transient splicing inhibition generates a window of vulnerability in HRP TNBC cells, which can be exploited therapeutically. Accordingly, the PdB pulse synergized with cisplatin and talazoparib, two drugs that are clinically approved for TNBC and display stronger effects in HRD patients.[3] This sequential treatment was effective in multiple HRP TNBC models, including two PDOs derived from neoadjuvant-insensitive tumors. Together, our findings suggest that transient splicing inhibition can be exploited to improve the efficacy of current treatments in patients who do not achieve pCRs.

Limitations of the study

Future studies will have to address whether transient splicing inhibition enhances chemotherapy response *in vivo* using mouse TNBC models. Moreover, since splicing inhibition also affects R loop formation and transcription-replication conflicts, we cannot rule out that site-specific R loop accumulation also contributes to DNA damage. However, since replication fork processing genes are downregulated by PdB, this issue is difficult to address.

RESOURCE AVAILABILITY

Lead contact

Requests for further information, resources, and reagents should be directed to and will be fulfilled by the lead contact, Claudio Sette (claudio.sette@unicatt.it).

Materials availability

Materials unique to this work, including three PDO lines, are available upon discussion and approval by the ethics committee (contact Claudio Sette: claudio.sette@unicatt.it).

(E) Heatmaps showing the mean values of survival of cells pre-treated for 6 h with PdB or DMSO followed by cisplatin (left) or talazoparib (right) at the indicated concentrations (n = 3). Scatter dot plots show the combination index (CI) for combined treatments with respect to individual treatments, calculated using CompuSyn software. CI < 1 indicates synergism.

(F) γH2AX (red) and Hoechst (blue) immunofluorescence staining of PDO-46 cultures pre-treated or not with 3.3 nM PdB (24 h) before carboplatin (33 μM, 24 h). Insets show the γH2AX foci in the dashed boxed cells (scale bar, 40 μm).

(G) Boxplots showing median and interquartile range of average γH2AX foci counted for each PDO treated as in (F). Error bars represent min and max value. The + symbol shows the mean value ($n \geq 10$, unpaired Student's t test with respect to DMSO [*] or between conditions [#]).

(H) PDO viability upon pre-treatment with PdB for 24 h before carboplatin (96 h) (mean ± SEM, $n \geq 5$, unpaired Student's t test with respect to DMSO [*] or between conditions [#]).

See also Figure S7.

Data and code availability

- RNA-seq data are available in the GEO database (GEO: GSE254842 and GSE271749).
- This paper does not report the original code.
- Any additional information required to reanalyze the data reported in this paper is available from the lead contact upon request.

ACKNOWLEDGMENTS

We thank Dr. Bonvissuto for IHC analysis, Dr. Guidi for cell sorting, Prof. Di Agostino for the gift of cell lines, and the GSTeP Organoids Facility of the IRCCS Fondazione Policlinico Gemelli for PDO development. This study was funded by Breast Cancer Now's Catalyst Program (grant ref. 2018NovPCC1283), which is supported by Pfizer, Associazione Italiana Ricerca sul Cancro (AIRC) grants IG23416 and MFAG21899, and Ministero della Salute Ricerca Corrente 2023. Università Cattolica del Sacro Cuore contributed to the funding of this research project and its publication.

AUTHOR CONTRIBUTIONS

Conceptualization, C.S., C.C., and C.N.; writing – original draft and review & editing, C.S. and C.C.; investigation, C.C., V.P., M.F., M.P., and E.C.; data curation, C.C., A.D.L., M.A.S., A.F., and R.M.; supervision, C.S.; funding acquisition, C.S. and C.N. The authors read and approved the final manuscript.

DECLARATION OF INTERESTS

The authors declare no competing interests.

STAR★METHODS

Detailed methods are provided in the online version of this paper and include the following:

- KEY RESOURCES TABLE
- EXPERIMENTAL MODEL AND STUDY PARTICIPANT DETAILS
  - Patient-derived organoids culture and viability assays
  - Cell culture and viability assays
- METHOD DETAILS
  - Extraction of RNA, RT-PCR and real-time PCR analysis
  - RNA-seq and bioinformatics analyses
  - Cell fractionation, isolation of chromatin-associated RNA and polysome profiling
  - Protein extracts and western blot analysis
  - Immunofluorescence assays
  - Flow cytometric analysis of phosphorylated histone H2AX
  - Cytofluorimetric sorting of MDA-MB-231 cells
  - Immunohistochemical analysis
- QUANTIFICATION AND STATISTICAL ANALYSIS

SUPPLEMENTAL INFORMATION

Supplemental information can be found online at https://doi.org/10.1016/j.celrep.2024.114751.

Received: February 20, 2024
Revised: July 17, 2024
Accepted: August 29, 2024
Published: September 13, 2024

REFERENCES

1. Loibl, S., Weber, K.E., Timms, K.M., Elkin, E.P., Hahnen, E., Fasching, P.A., Lederer, B., Denkert, C., Schneeweiss, A., Braun, S., et al. (2018). Survival analysis of carboplatin added to an anthracycline/taxane-based neoadjuvant chemotherapy and HRD score as predictor of response—final results from GeparSixto. Ann. Oncol. *29*, 2341–2347. https://doi.org/10.1093/annonc/mdy460.
2. Nolan, E., Lindeman, G.J., and Visvader, J.E. (2023). Deciphering breast cancer: from biology to the clinic. Cell *186*, 1708–1728. https://doi.org/10.1016/j.cell.2023.01.040.
3. Bianchini, G., De Angelis, C., Licata, L., and Gianni, L. (2022). Treatment landscape of triple-negative breast cancer — expanded options, evolving needs. Nat. Rev. Clin. Oncol. *19*, 91–113. https://doi.org/10.1038/s41571-021-00565-2.
4. Garrido-Castro, A.C., Lin, N.U., and Polyak, K. (2019). Insights into Molecular Classifications of Triple-Negative Breast Cancer: Improving Patient Selection for Treatment. Cancer Discov. *9*, 176–198. https://doi.org/10.1158/2159-8290.CD-18-1177.
5. Duijf, P.H.G., Nanayakkara, D., Nones, K., Srihari, S., Kalimutho, M., and Khanna, K.K. (2019). Mechanisms of Genomic Instability in Breast Cancer. Trends Mol. Med. *25*, 595–611. https://doi.org/10.1016/j.molmed.2019.04.004.
6. Groelly, F.J., Fawkes, M., Dagg, R.A., Blackford, A.N., and Tarsounas, M. (2023). Targeting DNA damage response pathways in cancer. Nat. Rev. Cancer *23*, 78–94. https://doi.org/10.1038/s41568-022-00535-5.
7. Litton, J.K., Hurvitz, S.A., Mina, L.A., Rugo, H.S., Lee, K.-H., Gonçalves, A., Diab, S., Woodward, N., Goodwin, A., Yerushalmi, R., et al. (2020). Talazoparib versus chemotherapy in patients with germline BRCA1/2-mutated HER2-negative advanced breast cancer: final overall survival results from the EMBRACA trial. Ann. Oncol. *31*, 1526–1535. https://doi.org/10.1016/j.annonc.2020.08.2098.
8. GSK (2022). Dear Health Care Provider Letter (Niraparib). https://www.zejulahcp.com/content/dam/cf-pharma/hcp-zejulahcp-v2/en_US/pdf/ZEJULA%20(niraparib)%20Dear%20HCP%20Letter%20November%202022.pdf.
9. Paulsen, R.D., Soni, D.V., Wollman, R., Hahn, A.T., Yee, M.-C., Guan, A., Hesley, J.A., Miller, S.C., Cromwell, E.F., Solow-Cordero, D.E., et al. (2009). A Genome-wide siRNA Screen Reveals Diverse Cellular Processes and Pathways that Mediate Genome Stability. Mol. Cell *35*, 228–239. https://doi.org/10.1016/j.molcel.2009.06.021.
10. Adamson, B., Smogorzewska, A., Sigoillot, F.D., King, R.W., and Elledge, S.J. (2012). A genome-wide homologous recombination screen identifies the RNA-binding protein RBMX as a component of the DNA-damage response. Nat. Cell Biol. *14*, 318–328. https://doi.org/10.1038/ncb2426.
11. Herr, P., Lundin, C., Evers, B., Ebner, D., Bauerschmidt, C., Kingham, G., Palmai-Pallag, T., Mortusewicz, O., Frings, O., Sonnhammer, E., and Helleday, T. (2015). A genome-wide IR-induced RAD51 foci RNAi screen identifies CDC73 involved in chromatin remodeling for DNA repair. Cell Discov. *1*, 15034. https://doi.org/10.1038/celldisc.2015.34.
12. Tholen, J., and Galej, W.P. (2022). Structural studies of the spliceosome: Bridging the gaps. Curr. Opin. Struct. Biol. *77*, 102461. https://doi.org/10.1016/j.sbi.2022.102461.
13. Bonnal, S.C., López-Oreja, I., and Valcárcel, J. (2020). Roles and mechanisms of alternative splicing in cancer — implications for care. Nat. Rev. Clin. Oncol. *17*, 457–474. https://doi.org/10.1038/s41571-020-0350-x.
14. Sette, C., and Paronetto, M.P. (2022). Somatic Mutations in Core Spliceosome Components Promote Tumorigenesis and Generate an Exploitable Vulnerability in Human Cancer. Cancers *14*, 1827. https://doi.org/10.3390/cancers14071827.
15. Stanley, R.F., and Abdel-Wahab, O. (2022). Dysregulation and therapeutic targeting of RNA splicing in cancer. Nat. Can. (Ott.) *3*, 536–546. https://doi.org/10.1038/s43018-022-00384-z.
16. Stricker, T.P., Brown, C.D., Bandlamudi, C., McNerney, M., Kittler, R., Montoya, V., Peterson, A., Grossman, R., and White, K.P. (2017). Robust stratification of breast cancer subtypes using differential patterns of transcript isoform expression. PLoS Genet. *13*, e1006589. https://doi.org/10.1371/journal.pgen.1006589.

17. Ke, H., Zhao, L., Zhang, H., Feng, X., Xu, H., Hao, J., Wang, S., Yang, Q., Zou, L., Su, X., et al. (2018). Loss of TDP43 inhibits progression of triple-negative breast cancer in coordination with SRSF3. Proc. Natl. Acad. Sci. USA *115*, E3426–E3435. https://doi.org/10.1073/pnas.1714573115.

18. Cieśla, M., Ngoc, P.C.T., Cordero, E., Martinez, Á.S., Morsing, M., Muthukumar, S., Beneventi, G., Madej, M., Munita, R., Jönsson, T., et al. (2021). Oncogenic translation directs spliceosome dynamics revealing an integral role for SF3A3 in breast cancer. Mol. Cell *81*, 1453–1468.e12. https://doi.org/10.1016/j.molcel.2021.01.034.

19. Naro, C., De Musso, M., Delle Monache, F., Panzeri, V., de la Grange, P., and Sette, C. (2021). The oncogenic kinase NEK2 regulates an RBFOX2-dependent pro-mesenchymal splicing program in triple-negative breast cancer cells. J. Exp. Clin. Cancer Res. *40*, 397. https://doi.org/10.1186/s13046-021-02210-3.

20. Bland, P., Saville, H., Wai, P.T., Curnow, L., Muirhead, G., Nieminuszczy, J., Ravindran, N., John, M.B., Hedayat, S., Barker, H.E., et al. (2023). SF3B1 hotspot mutations confer sensitivity to PARP inhibition by eliciting a defective replication stress response. Nat. Genet. *55*, 1311–1323. https://doi.org/10.1038/s41588-023-01460-5.

21. Bakhoum, S.F., and Cantley, L.C. (2018). The Multifaceted Role of Chromosomal Instability in Cancer and Its Microenvironment. Cell *174*, 1347–1360. https://doi.org/10.1016/j.cell.2018.08.027.

22. Mateo, J., Lord, C.J., Serra, V., Tutt, A., Balmaña, J., Castroviejo-Bermejo, M., Cruz, C., Oaknin, A., Kaye, S.B., and de Bono, J.S. (2019). A decade of clinical development of PARP inhibitors in perspective. Ann. Oncol. *30*, 1437–1447. https://doi.org/10.1093/annonc/mdz192.

23. Bartkova, J., Tommiska, J., Oplustilova, L., Aaltonen, K., Tamminen, A., Heikkinen, T., Mistrik, M., Aittomäki, K., Blomqvist, C., Heikkilä, P., et al. (2008). Aberrations of the MRE11–RAD50–NBS1 DNA damage sensor complex in human breast cancer: *MRE11* as a candidate familial cancer-predisposing gene. Mol. Oncol. *2*, 296–316. https://doi.org/10.1016/j.molonc.2008.09.007.

24. Nagelkerke, A., van Kuijk, S.J.A., Sweep, F.C.G.J., Nagtegaal, I.D., Hoogerbrugge, N., Martens, J.W.M., Timmermans, M.A., van Laarhoven, H.W.M., Bussink, J., and Span, P.N. (2011). Constitutive expression of γ-H2AX has prognostic relevance in triple negative breast cancer. Radiother. Oncol. *101*, 39–45. https://doi.org/10.1016/j.radonc.2011.07.009.

25. Peng, J., Tang, L., Cai, M., Chen, H., Wong, J., and Zhang, P. (2019). RECQL5 plays an essential role in maintaining genome stability and viability of triple-negative breast cancer cells. Cancer Med. *8*, 4743–4752. https://doi.org/10.1002/cam4.2349.

26. Lehmann, B.D., Bauer, J.A., Chen, X., Sanders, M.E., Chakravarthy, A.B., Shyr, Y., and Pietenpol, J.A. (2011). Identification of human triple-negative breast cancer subtypes and preclinical models for selection of targeted therapies. J. Clin. Invest. *121*, 2750–2767. https://doi.org/10.1172/JCI45014.

27. Kastner, B., Will, C.L., Stark, H., and Lührmann, R. (2019). Structural Insights into Nuclear pre-mRNA Splicing in Higher Eukaryotes. Cold Spring Harbor Perspect. Biol. *11*, a032417. https://doi.org/10.1101/cshperspect.a032417.

28. Bonnal, S., Vigevani, L., and Valcárcel, J. (2012). The spliceosome as a target of novel antitumour drugs. Nat. Rev. Drug Discov. *11*, 847–859. https://doi.org/10.1038/nrd3823.

29. Kotake, Y., Sagane, K., Owa, T., Mimori-Kiyosue, Y., Shimizu, H., Uesugi, M., Ishihama, Y., Iwata, M., and Mizui, Y. (2007). Splicing factor SF3b as a target of the antitumor natural product pladienolide. Nat. Chem. Biol. *3*, 570–575. https://doi.org/10.1038/nchembio.2007.16.

30. Chang, A.Y., Zhou, Y.J., Iyengar, S., Pobiarzyn, P.W., Tishchenko, P., Shah, K.M., Wheeler, H., Wang, Y.-M., Loria, P.M., Loganzo, F., and Woo, S.R. (2021). Modulation of SF3B1 in the pre-mRNA spliceosome induces a RIG-I-dependent type I IFN response. J. Biol. Chem. *297*, 101277. https://doi.org/10.1016/j.jbc.2021.101277.

31. Ghosh, A.K., Veitschegger, A.M., Nie, S., Relitti, N., MacRae, A.J., and Jurica, M.S. (2018). Enantioselective Synthesis of Thailanstatin A Methyl Ester and Evaluation of *in Vitro* Splicing Inhibition. J. Org. Chem. *83*, 5187–5198. https://doi.org/10.1021/acs.joc.8b00593.

32. Han, T., Goralski, M., Gaskill, N., Capota, E., Kim, J., Ting, T.C., Xie, Y., Williams, N.S., and Nijhawan, D. (2017). Anticancer sulfonamides target splicing by inducing RBM39 degradation via recruitment to DCAF15. Science *356*, eaal3755. https://doi.org/10.1126/science.aal3755.

33. Elstrodt, F., Hollestelle, A., Nagel, J.H.A., Gorin, M., Wasielewski, M., van den Ouweland, A., Merajver, S.D., Ethier, S.P., and Schutte, M. (2006). BRCA1 Mutation Analysis of 41 Human Breast Cancer Cell Lines Reveals Three New Deleterious Mutants. Cancer Res. *66*, 41–45. https://doi.org/10.1158/0008-5472.CAN-05-2853.

34. Hustedt, N., and Durocher, D. (2016). The control of DNA repair by the cell cycle. Nat. Cell Biol. *19*, 1–9. https://doi.org/10.1038/ncb3452.

35. Cesari, E., Ciucci, A., Pieraccioli, M., Caggiano, C., Nero, C., Bonvissuto, D., Sillano, F., Buttarelli, M., Piermattei, A., Loverro, M., et al. (2023). Dual inhibition of CDK12 and CDK13 uncovers actionable vulnerabilities in patient-derived ovarian cancer organoids. J. Exp. Clin. Cancer Res. *42*, 126. https://doi.org/10.1186/s13046-023-02682-5.

36. Huen, M.S.Y., Grant, R., Manke, I., Minn, K., Yu, X., Yaffe, M.B., and Chen, J. (2007). RNF8 Transduces the DNA-Damage Signal via Histone Ubiquitylation and Checkpoint Protein Assembly. Cell *131*, 901–914. https://doi.org/10.1016/j.cell.2007.09.041.

37. Caizzi, L., Monteiro-Martins, S., Schwalb, B., Lysakovskaia, K., Schmitzova, J., Sawicka, A., Chen, Y., Lidschreiber, M., and Cramer, P. (2021). Efficient RNA polymerase II pause release requires U2 snRNP function. Mol. Cell *81*, 1920–1934.e9. https://doi.org/10.1016/j.molcel.2021.02.016.

38. Sousa-Luís, R., Dujardin, G., Zukher, I., Kimura, H., Weldon, C., Carmo-Fonseca, M., Proudfoot, N.J., and Nojima, T. (2021). POINT technology illuminates the processing of polymerase-associated intact nascent transcripts. Mol. Cell *81*, 1935–1950.e6. https://doi.org/10.1016/j.molcel.2021.02.034.

39. Nie, C., Zhou, X.A., Zhou, J., Liu, Z., Gu, Y., Liu, W., Zhan, J., Li, S., Xiong, Y., Zhou, M., et al. (2023). A transcription-independent mechanism determines rapid periodic fluctuations of BRCA1 expression. EMBO J. *42*, e111951. https://doi.org/10.15252/embj.2022111951.

40. Senft, D., Qi, J., and Ronai, Z.A. (2018). Ubiquitin ligases in oncogenic transformation and cancer therapy. Nat. Rev. Cancer *18*, 69–88. https://doi.org/10.1038/nrc.2017.105.

41. Litton, J.K., Rugo, H.S., Ettl, J., Hurvitz, S.A., Gonçalves, A., Lee, K.-H., Fehrenbacher, L., Yerushalmi, R., Mina, L.A., Martin, M., et al. (2018). Talazoparib in Patients with Advanced Breast Cancer and a Germline *BRCA* Mutation. N. Engl. J. Med. *379*, 753–763. https://doi.org/10.1056/NEJMoa1802905.

42. Foukakis, T. (2018). Carboplatin in the neoadjuvant treatment of triple-negative breast cancer—ready for prime time? Ann. Oncol. *29*, 2278–2280. https://doi.org/10.1093/annonc/mdy494.

43. Loibl, S., Poortmans, P., Morrow, M., Denkert, C., and Curigliano, G. (2021). Breast cancer. Lancet *397*, 1750–1769. https://doi.org/10.1016/S0140-6736(20)32381-3.

44. Chan, Y.A., Hieter, P., and Stirling, P.C. (2014). Mechanisms of genome instability induced by RNA-processing defects. Trends Genet. *30*, 245–253. https://doi.org/10.1016/j.tig.2014.03.005.

45. Naro, C., Bielli, P., Pagliarini, V., and Sette, C. (2015). The interplay between DNA damage response and RNA processing: the unexpected role of splicing factors as gatekeepers of genome stability. Front. Genet. *6*, 142. https://doi.org/10.3389/fgene.2015.00142.

46. Carey, K.T., and Wickramasinghe, V.O. (2018). Regulatory Potential of the RNA Processing Machinery: Implications for Human Disease. Trends Genet. *34*, 279–290. https://doi.org/10.1016/j.tig.2017.12.012.

47. Paronetto, M.P., Miñana, B., and Valcárcel, J. (2011). The Ewing Sarcoma Protein Regulates DNA Damage-Induced Alternative Splicing. Mol. Cell *43*, 353–368. https://doi.org/10.1016/j.molcel.2011.05.035.

48. Savage, K.I., Gorski, J.J., Barros, E.M., Irwin, G.W., Manti, L., Powell, A.J., Pellagatti, A., Lukashchuk, N., McCance, D.J., McCluggage, W.G., et al. (2014). Identification of a BRCA1-mRNA Splicing Complex Required for Efficient DNA Repair and Maintenance of Genomic Stability. Mol. Cell *54*, 445–459. https://doi.org/10.1016/j.molcel.2014.03.021.

49. Chen, L., Chen, J.-Y., Huang, Y.-J., Gu, Y., Qiu, J., Qian, H., Shao, C., Zhang, X., Hu, J., Li, H., et al. (2018). The Augmented R-Loop Is a Unifying Mechanism for Myelodysplastic Syndromes Induced by High-Risk Splicing Factor Mutations. Mol. Cell *69*, 412–425.e6. https://doi.org/10.1016/j.molcel.2017.12.029.

50. Lappin, K.M., Barros, E.M., Jhujh, S.S., Irwin, G.W., McMillan, H., Liberante, F.G., Latimer, C., La Bonte, M.J., Mills, K.I., Harkin, D.P., et al. (2022). Cancer-Associated SF3B1 Mutations Confer a BRCA-Like Cellular Phenotype and Synthetic Lethality to PARP Inhibitors. Cancer Res. *82*, 819–830. https://doi.org/10.1158/0008-5472.CAN-21-1843.

51. McGrail, D.J., Li, Y., Smith, R.S., Feng, B., Dai, H., Hu, L., Dennehey, B., Awasthi, S., Mendillo, M.L., Sood, A.K., et al. (2023). Widespread BRCA1/2-independent homologous recombination defects are caused by alterations in RNA-binding proteins. Cell Rep. Med. *4*, 101255. https://doi.org/10.1016/j.xcrm.2023.101255.

52. Steensma, D.P., Wermke, M., Klimek, V.M., Greenberg, P.L., Font, P., Komrokji, R.S., Yang, J., Brunner, A.M., Carraway, H.E., Ades, L., et al. (2021). Phase I First-in-Human Dose Escalation Study of the oral SF3B1 modulator H3B-8800 in myeloid neoplasms. Leukemia *35*, 3542–3550. https://doi.org/10.1038/s41375-021-01328-9.

53. Hsu, T.Y.-T., Simon, L.M., Neill, N.J., Marcotte, R., Sayad, A., Bland, C.S., Echeverria, G.V., Sun, T., Kurley, S.J., Tyagi, S., et al. (2015). The spliceosome is a therapeutic vulnerability in MYC-driven cancer. Nature *525*, 384–388. https://doi.org/10.1038/nature14985.

54. Koh, C.M., Bezzi, M., Low, D.H.P., Ang, W.X., Teo, S.X., Gay, F.P.H., Al-Haddawi, M., Tan, S.Y., Osato, M., Sabò, A., et al. (2015). MYC regulates the core pre-mRNA splicing machinery as an essential step in lymphomagenesis. Nature *523*, 96–100. https://doi.org/10.1038/nature14351.

55. Wheeler, E.C., Martin, B.J.E., Doyle, W.C., Neaher, S., Conway, C.A., Pitton, C.N., Gorelov, R.A., Donahue, M., Jann, J.C., Abdel-Wahab, O., et al. (2024). Splicing modulators impair DNA damage response and induce killing of cohesin-mutant MDS and AML. Sci. Transl. Med. *16*, eade2774. https://doi.org/10.1126/scitranslmed.ade2774.

56. Krajewska, M., Dries, R., Grassetti, A.V., Dust, S., Gao, Y., Huang, H., Sharma, B., Day, D.S., Kwiatkowski, N., Pomaville, M., et al. (2019). CDK12 loss in cancer cells affects DNA damage response genes through premature cleavage and polyadenylation. Nat. Commun. *10*, 1757. https://doi.org/10.1038/s41467-019-09703-y.

57. da Costa, A.A.B.A., Chowdhury, D., Shapiro, G.I., D'Andrea, A.D., and Konstantinopoulos, P.A. (2023). Targeting replication stress in cancer therapy. Nat. Rev. Drug Discov. *22*, 38–58. https://doi.org/10.1038/s41573-022-00558-5.

58. Harris, P.A., Taylor, R., Thielke, R., Payne, J., Gonzalez, N., and Conde, J.G. (2009). Research electronic data capture (REDCap)—A metadata-driven methodology and workflow process for providing translational research informatics support. J. Biomed. Inf. *42*, 377–381. https://doi.org/10.1016/j.jbi.2008.08.010.

59. Lehmann, B.D., Colaprico, A., Silva, T.C., Chen, J., An, H., Ban, Y., Huang, H., Wang, L., James, J.L., Balko, J.M., et al. (2021). Multi-omics analysis identifies therapeutic vulnerabilities in triple-negative breast cancer subtypes. Nat. Commun. *12*, 6276. https://doi.org/10.1038/s41467-021-26502-6.

STAR★METHODS

KEY RESOURCES TABLE

REAGENT or RESOURCE	SOURCE	IDENTIFIER
Antibodies		
Anti-γH2AX	Cell signaling	Cat#9718; RRID AB_2118009
Anti-cyclin A	Santa Cruz Biotechnology	Cat # 271645 RRID AB_10707658
Anti-cyclin A2	Proteintech	Cat # 66391 RRID: AB_2881767
Anti-cyclin B1	Santa Cruz Biotechnology	Cat # sc-245 RRID:AB_627338
Anti-cyclin E2	Cell signaling	Cat # 4132 RRID:AB_2071197
Anti-BRCA1	Cell signaling	Cat#9010; RRID AB_2228244
Anti-BRCA2	Calbiochem	Cat#OP95; RRID AB_2067762
Anti-ATRIP	Cell signaling	Cat#2737; RRID AB_823659
Anti-RNF8	Santa Cruz Biotechnology	Cat#sc-271462; RRID AB_10648902
Anti-RAD51	Calbiochem	Cat# pc130; RRID AB_2238184
Anti- ACTB	Santa Cruz Biotechnology	Cat#sc-47778; RRID AB_626632
Anti-GAPDH	Santa Cruz Biotechnology	Cat#sc-32233; RRID AB_627679
Anti-H3	Proteintech	Cat # 17168-1-AP, RRID AB_2716755
Anti-DDX21	Santa Cruz Biotechnology	Cat#sc-376953; RRID AB_2819085
Anti-CDK7	Cell signaling	Cat#2916; RRID AB_2077142
Anti-FIP1L1	Bethyl	Cat#A301-462; RRID AB_999566
Anti-CHEK1	Cell signaling	Cat#2360; RRID AB_2080320
Anti-phospho-CHEK1	Cell signaling	Cat#2349; RRID AB_2080323
Anti-PARP1	Cell signaling	Cat#9542S; RRID AB_2160739
Anti-Ki-67	Abcam	Cat#ab16667; RRID AB_302459
Anti-ER	Abcam	Cat#ab16660; RRID AB_443420
Anti-PR	Abcam	Cat#ab16661; RRID AB_443421
Anti-Her2	Abcam	Cat # ab231438, RRID AB_3086651
Anti-mouse Alexa Fluor 594	Thermo Fisher Scientific	Cat # A11005, RRID AB_2534073
Anti-rabbit Alexa Fluor 488	Thermo Fisher Scientific	Cat # A11008, RRID AB_143165
Anti-rabbit Alexa Fluor 594	Thermo Fisher Scientific	Cat # A11037, RRID AB_2534095

(*Continued on next page*)

Continued

REAGENT or RESOURCE	SOURCE	IDENTIFIER
Biological samples		
Tumor biopsies	This study	N/A
Chemicals, peptides, and recombinant proteins		
RPMI 1640	Euroclone	Cat # ECM2001L
Fetal bovine serum (FBS)	Thermo Fisher Scientific	Cat # 10270-106
Penicillin and streptomycin	Aurogene	Cat # AU-L0022-100
HEPES for cell culture	Gibco	Cat # 15630-106
Sodium Pyruvate for cell culture	Gibco	Cat # 11360-070
Glucose for cell culture	Biowest	Cat #P5030
Protease-Inhibitor Cocktail	Sigma-Aldrich	Cat #P8340
DTT, Dithiothreitol	Panreac AppliChem	Cat # A2948
Sodium orthovanadate	Enzo	Cat # ALX-400-032
37% formaldehyde	Sigma-Aldrich	Cat #F8775
8% paraformaldehyde	Alfa Aesar	Cat # 47347
Triton X-100	Sigma Aldrich	Cat #T8787
NP-40	Applichem	Cat # A1694
Sucrose	Sigma-Aldrich	Cat # 16104
EDTA (Ethylenediaminetetraacetic acid disodium salt)	Sigma-Aldrich	Cat #E5134
Tris Base	VWR Life Science	Cat # 0826
Sodium chloride	Applichem	Cat # A2942
HEPES	Sigma-Aldrich	Cat #H4034
Magnesium chloride	Sigma-Aldrich	Cat #M2670
PMSF Protease Inhibitor	Sigma-Aldrich	Cat #P7626
Glycerol	Sigma-Aldrich	Cat #G7757
RNasin	Promega	Cat #N251B
Urea	Eurobio	Cat # 018228
Nonfat dried milk powder	Applichem	Cat # A0830
BSA for molecular biology	VWR Life Science	Cat # 422361V
Ponceau S	Sigma-Aldrich	Cat #P7170
M-MLV reverse transcriptase	Promega	Cat #M1705
Random hexamers	Roche	Cat # 11034731001
Oligo(dT)15 Primer	Promega	Cat #C1101
dNTPs	Promega	Cat #U1245
GoTaq	Promega	Cat #M7845
PowerUP SYBR Green Master Mix	Thermo Fisher Scientific	Cat # A25777
Crystal violet	Sigma-Aldrich	Cat #C3886-100G
Dmso	Applichem	Cat # A3672,0100
Carboplatin	Selleckchem	Cat #S1215
Cisplatin	Selleckchem	Cat #S1166
Talazoparib	Pfizer	CAS number 1373431-65-2
Pladienolide B	Santa Cruz Biotechnology	Cat # 391691
Thailanstatin A	MedChemExpress	Cat # HY-129589
Indisulam	MedChemExpress	Cat # HY-13650
MG132	MedChemExpress	Cat # HY-13259
Mimosine	Sigma-Aldrich	Cat #M0253
7-AAD	Biotium	Cat # 40037
Propidium iodide	Sigma-Aldrich	Cat #P4170
DRB, 5,6-dichlorobenzimidazole	Sigma-Aldrich	Cat #D1916

(*Continued on next page*)

Continued

REAGENT or RESOURCE	SOURCE	IDENTIFIER
Cycloheximide	Sigma-Aldrich	Cat #c1988
Triton X-100	Sigma-Aldrich	Cat #X100-12
Tween 20	Sigma-Aldrich	Cat #P1379
Horse serum	Sigma-Aldrich	Cat # 12449C
Hoechst 33342	Thermo Fisher Scientific	Cat #H3570
Incucyte® Cytotox Green Dye	Sartorius	Cat # 4633
Advanced DMEM/F-12	Thermo Fisher Scientific	Cat # 12634-010
Glutamax	Thermo Fisher Scientific	Cat # 35050038
DPBS	Euroclone	Cat # ECB4004L
B27	Thermo Fisher Scientific	Cat # 17504-44
EGF	Peprotech	Cat # AF-100-15
Insulin	Roche	Cat # 11376497001
b-estradiol	Sigma-Aldrich	Cat #E8875
FGF7	Peprotech	Cat # 100-19
FGF10	Peprotech	Cat # 100-26
Forskolin	Tocris	Cat # 1099
Heregulin	Peprotech	Cat # 100-03
Hydrocortisone	Sigma-Aldrich	Cat #H0888
N-acetyl-L-cysteine	Sigma-Aldrich	Cat # A9165
Nicotinamide	Sigma-Aldrich	Cat #N0636
Noggin	Peprotech	Cat #120-10C
Primocin	Invivogen	Cat # ANT-PM-1
R-spondin	Conditioned medium from HEK-293	NA
SB202190	Sigma-Aldrich	Cat #S7067
Y27632	Tocris	Cat # 1254
Triple express	Thermo Fisher Scientific	Cat # 12605-028
Cultrex growth factor reduced BME type 2	Bio-Techne	Cat # 3533-010-02
Collagenase II	Thermo Fisher Scientific	Cat # 1701-015
Critical commercial assays		
TRIzol Reagent	Thermo Fisher Scientific	Cat # 15596018
RNEasy mini kit	Qiagen	Cat # 74104
TURBO DNA-free Kit	Thermo Fisher Scientific	Cat # AM1907
Bio-Rad protein assay	Bio-Rad	Cat # 5000006
Clarity Western ECL Blotting Substrate	Bio-Rad	Cat # 1705061
RNeasy Mini Kit	Qiagen	Cat # 74904
CellTiter-Glo® Luminescent Cell Viability Assay	Promega	Cat #G9681
Red Blood cell lysis	Roche	Cat # 11814389001
Deposited data		
Fraction of genome altered from human BC tumors	The Cancer Genome Atlas, Firehose Legacy	TCGA, Breast Cancer
Genomic instability index	The Clinical Proteomic Tumor Analysis Consortium	CPTAC, Breast cancer
Genes involved in genome stabilization by monitoring phosphorylation of the histone variant H2AX	http://www.sciencedirect.com/science/journal/10972765	Paulsen et al.[9]
Genes involved in the regulation of homologous recombination by monitoring RAD51 foci formation upon irradiation	http://www.nature.com/celldisc/	Herr et al.[11]
Genes involved in the regulation of homologous recombination using a GFP-based reporter	http://www.nature.com/ncb/	Adamson et al.[10]

(*Continued on next page*)

Continued

REAGENT or RESOURCE	SOURCE	IDENTIFIER
RNA-seq data from MDA-MB-231 cell line	This study	GEO: GSE254842
RNA-seq data from MDA-MB-231 cell line	This study	GEO: GSE271749
Experimental models: Cell lines		
MDA-MB-231 cell line	ATCC	HTB-26
MDA-MB-436 cell line	ATCC	HTB-130
HCC1806 cell line	ATCC	CRL-2335
MCF10A	Gift from Prof. Silvia Di Agostino	N/A
HBL-100	Gift from Prof. Silvia Di Agostino	N/A
SK-BR-3	Gift from Prof. Silvia Di Agostino	N/A
ZR-75-I	Gift from Prof. Silvia Di Agostino	N/A
T-47D	Gift from Prof. Silvia Di Agostino	N/A
Experimental models: Patient-derived organoids		
TNBC organoids	This study	N/A
Oligonucleotides		
See Table S6 for oligonucleotide sequences used in this study	This study	N/A
Software and algorithms		
cBioPortal	Memorial Sloan Kettering Cancer Center	www.cbioportal.org
CytExpert software v2.4.0.28	Beckman Coulter	N/A
ImageJ software V2.0.0-rc-69/1.52p	NIH	https://imagej.net/Contributors
GraphPad Software		https://www.graphpad.com/
Image Lab	Biorad	https://www.bio-rad.com/it-it/product/image-lab-software?ID=KRE6P5E8Z
Compusyn v1.0	Chou–Talalay method, 2004	N/A
R V4.3.0	CRAN	www.cran.r-project.org/
FastQC V.0.11.9	Babraham Institute Bioinformatics Group	https://www.bioinformatics.babraham.ac.uk/projects/fastqc
Picard V3.0.0	Broad Institute	https://broadinstitute.github.io/picard/
RSeQC V4.0.0		https://rseqc.sourceforge.net/
STAR V2.7.5.a		https://github.com/alexdobin/STAR
featureCounts V2.0.3		https://subread.sourceforge.net/
Genomation	Bioconductor	https://bioconductor.org/packages/release/bioc/html/genomation.html
ggplot2	CRAN	https://cran.r-project.org/web/packages/ggplot2/index.html
Other		
IncuCyte SX5 Live-content imaging system	Sartorius	N/A
SpectraMax QuickDrop Micro-Volume Spectrophotometer	Molecular Devices	N/A
CytoFlex flow cytometer	Beckman Coulter	N/A
QuantStudio™ 3 Real-Time PCR System	Applied biosystems	N/A
Zeiss Axiophot fluorescence microscope	Zeiss	N/A
Nikon Eclipse Ti2-inverted microscope	Nikon	N/A
BD FACSMelody™ Cell Sorter	BD Biosciences	N/A

EXPERIMENTAL MODEL AND STUDY PARTICIPANT DETAILS

Patient-derived organoids culture and viability assays

Tumor biopsies were collected from patients treated at ‘‘Fondazione Policlinico Universitario A. Gemelli IRCCS’’ (FPG), Rome, Italy, from May 2020 to October 2022. The protocol was approved by the Institutional Review Board (Protocol ID: 3642) and conducted in

accordance with the Helsinki Declaration. All patients enrolled gave their written informed consent for participation. Relevant clinical data were collected and managed using REDCap electronic data capture tools[58] at FPG (https://redcap-irccs.policlinicogemelli.it). Clinical information of patients enrolled for this study are listed in Table S5.

Breast cancer tissue were minced, washed with 10mL AdDF+++ (Advanced DMEM/F12 containing 1x Glutamax, 10mM HEPES, and antibiotics) and digested in 10mL of AdDF+++ containing 4 mg/ml collagenase II on an orbital shaker at 37°C for 1/2 h. The digested tissue suspension was sheared pipetting up and down 10 times and then was strained over a 100mm pre-coated (with PBS 0.1% BSA) filter and centrifugated at 490 rcf for 5 min. The pellet was resuspended in 10mL AdDF+++ and centrifuged again. In case of a visible red pellet, erythrocytes were lysed in 2mL red blood cell lysis buffer for 5 min before the addition of 10mL AdDF+++ and centrifugation at 490 rcf. The pellet was resuspended in 10 mg/ml of cold Cultrex growth factor reduced BME type 2 and 40mL drops of BME-cell suspension were allowed to solidify on prewarmed 24-well suspension culture plates at 37°C for 30 min. Upon completed gelation, 400μL of BC organoid medium (AdDF+++, 0.5μM A8301, 1X B27, 5 ng/ml EGF, 100nM b-estradiol, 5 ng/ml FGF7, 20 ng/ml FGF10, 10uM forskolin, 5nM heregulin b1, 0.5ug/ml hydrocortisone, 1.25mM N-Acetilcysteine, 10mM nicotinamide, 100 ng/ml noggin, 100 μg/ml primocin, 10% R-Spondin conditioned medium, 1μM SB202190, 5μM Y27632) was added to each well and plates transferred to humidified 37°C-5% CO_2 incubators. Medium was changed every 3 days and organoids were passaged every 1–4 weeks. For organoids splitting, cystic organoids were resuspended and incubated in 0.2mL pre-warmed Triple Express for 7–10 min and mechanically sheared pipetting up and down several times. Triple Express activity was blocked adding 10mL of AdDF+++ and centrifugation at 490 rcf. Organoid fragments were resuspended in cold BME and re-seeded as above at ratios (1:1 to 1:6) allowing the formation of new organoids.

For PDO viability assay, organoids were dissociated with Triple Express fragments and resuspended in 2% BME growth medium before seeding in 100μL volume on BME pre-coated 96-well plates. After 24 h, the cells were treated with the indicated drugs for 5 days and viability was determined by Cell Titer-Glo luminescent assay using the Spark multimode microplate reader. Drug dose–response curves were visualized using linear regression analysis using GraphPad Prism 9 and half-maximal inhibitory concentration (IC50) values were determined from fitting curves. Counting of organoids was performed using nine images for each treatment condition. PDOs were classified as small, medium, or large based on their diameter measured manually drawing lines with ImageJ software. To calculate the organoid diameter range, we subtracted the diameter of the smallest organoid from the diameter of the largest organoid and divided this value by 3. Then, the obtained value was used to determine the diameter range for small, medium, and large organoids.

Cell culture and viability assays

MDA-MB-231, MDA-MB-436, HCC1806, MCF10A, HBL-100, SK-BR-3, ZR-75-I and T-47D cells were grown in RPMI 1640, supplemented with 10% FBS, antibiotics, 4500 mg/L glucose, 10mM HEPES and 1mM sodium pyruvate. Additional growth supplements were 10 μg/ml insulin for MCF10A and T-47D, and 20 ng/ml EGF for MCF10A. Cells were seeded in 96-well plates and the next day incubated with the appropriate drugs. After the pulse with splicing inhibitors, the culture media was removed, cells were washed with DPBS and grown in normal growth media as indicated. For crystal violet assay, the medium was discarded after 6 days, cells were washed with PBS and dried under fume hood. A total of 100μL of crystal violet solution (0.2% in H_2O) was added in each well and after 30 min the plate was washed with distilled water. Dried plates were used to measure the OD of each well using a plate reader (OD570 nm). For cell proliferation and death assays the cells were labeled with Cytotox Green Dye, incubated in the IncuCyte SX5 Live-content imaging system at 37°C with 5% CO_2 and imaged at 10X magnification every 12 h for 96 h (four images/well). Analysis was preformed using the Cell-by-Cell software to detect and quantify live and dead cells.

METHOD DETAILS

Extraction of RNA, RT-PCR and real-time PCR analysis

RNA was extracted using Trizol reagent and treated with TURBO DNA-free Kit. RNA purity and concentration were quantified using spectrophotometer and 1μg of RNA was retrotranscribed using M-MLV reverse transcriptase and oligo(dT) to test the transcript levels or random hexamers to test intron retention and snRNA levels. 20 ng of cDNA was used as template for PCR analyzed on agarose gels. Quantitative real-time PCRs (qPCR) were performed using QuantStudio 3 Real-Time PCR System and PowerUP SYBR Green Master Mix. Gene expression levels were analyzed respect to TUBA4A as reference gene using $2^{-\Delta Ct}$ method. The splicing of first introns was analyzed respect to processed region of the transcript. Oligonucleotides used are listed in Table S6.

RNA-seq and bioinformatics analyses

For RNA-seq analysis, total RNA was extracted and DNase-treated using the RNeasy Mini Kit from MDA-MB-231 cells treated with 10nM PdB or Dmso for 6 h. PolyA plus RNA-seq libraries were constructed and sequenced using a 150bp paired-end format on an Illumina NovaSeq6000 (GSE254842). RNA-seq data analysis was performed as previously described.[19] Briefly, sequencing, data quality, reads repartition (e.g., for potential ribosomal contamination), inner distance size estimation, genebody coverage, strand-specificity of library were performed using FastQC v0.11.2, Picard-Tools v1.119, Samtools v1.0 and RSeQC v2.3.9. Reads were mapped using STARv2.7.5a on the human hg38 genome assembly and read count was performed using featureCount from SubRead. Analysis at gene expression level was performed using Human FAST DB v2021_3 annotation[35] and DESeq2. Differential

expressed genes were considered statistically significant for p-values ≤ 0.05 and fold-changes ≥ 1.5. Splicing analyses were performed using "EXON" and "PATTERN" analyses as previously described[35] and results were considered statistically significant for p-values ≤ 0.05 and fold-changes ≥ 1.5. For RNA-seq analysis of MDA-MB-231 cells treated with 10nM PdB or Dmso for 16 h and recovered 24 h after PdB removal, the PolyA plus RNA-seq libraries were constructed and sequenced using a 101bp paired-end format on an Illumina NovaSeq6000 (GSE271749).

Gene metaprofiles were created by dividing each gene from transcription star site (TSS) to transcription end site (TES) into 50 equally sized bins. Bam files were used to calculate read coverage (read counts per million mapped reads) between downregulated or splicing-regulated genes in cells treated with PdB or Dmso in strand aware mode using 'Genomation' package in R. To account for the differential gene expression, reads counts were rescaled as percentage of mapped reads and their distribution within the gene body was drawn using 'ggplot2' package in R.

Gene Ontology (GO) analysis for cellular component of common genes between 'Factors maintaining genome stability', 'Positive regulators of HR' and 'Positive regulators of HR after IR', and GO for biological processes of downregulated genes was performed using 'TopGO' package using modified elim Fisher's test in R.

Expression levels, number of exons for gene, mean exons and introns lengths and gene lengths for genes related or not to DDR were evaluated and represented using custom R script.

Fraction of genome altered and Chromosome INstability index (CIN) analyses in TNBC and other BC were performed using the TGCA and CPTAC datasets from the cBioPortal database using the classification provided by Lehmann et al.[59]

Cell fractionation, isolation of chromatin-associated RNA and polysome profiling

For nucleus/cytoplasm fractionation, plasma membranes were lysed in the buffer (10mM Tris-HCl pH 7.5, 0.5% NP40 and 150mM NaCl) supplemented with 2mM Na-orthovanadate, 1mM DTT and protease-inhibitor cocktail. After 10 min, the lysate was then layered on top of 2.5 volumes of a chilled sucrose cushion (24% sucrose in lysis buffer) and centrifuged for 10 min, 4°C, 14,000 rpm. The cytoplasmic RNA was extracted from supernatant using 2 volumes of Trizol. The nuclei pellet was gently rinsed and then re-suspended in Trizol.

For chromatin-associated RNA isolation, cell pellets were re-suspended in the 1st buffer (20mM HEPES pH7.5, 10mM KCl, 5mM $MgCl_2$, 1mM EDTA, 250mM sucrose) supplemented with 1 mM PMSF, 2mM Na-orthovanadate, 1mM DTT, NaF 5mM and protease-inhibitors and lysed by the addition of Triton X-100 to 1% final concentration (10 min, 4°C). Nuclei were pelleted by centrifugation (650g, 5 min) and re-suspended in 2nd buffer (20mM HEPES pH7.5, 10mM KCl, 5mM $MgCl_2$, 1mM EDTA, 250mM sucrose) supplemented with RNasin (1:1000), 1mM PMSF, 2mM Na-orthovanadate, 5mM NaF and protease-inhibitors. The chromatin was extracted for 10 min at 4°C by the addition of ten volumes of 3rd buffer (20mM HEPES pH7.5, 10mM KCl, 5mM $MgCl_2$, 1mM EDTA, 250mM sucrose) supplemented with RNasin, 1M urea, 2mM Na-orthovanadate, 5mM NaF, 1mM DTT and protease-inhibitors. The chromatin was sedimented by centrifugation (15,000 x g at 4°C) and the RNA was extracted using Trizol.

For polysome fractionation, cells were homogenized in lysis buffer (30mM Tris-HCl pH 7.5, 100mM NaCl, 10mM $MgCl_2$, 1mM DTT, 30 U ml−1 RNasin, 0.5% Triton X-100, 2mM Na-orthovanadate and protease-inhibitors) supplemented with 100 μg/ml cycloheximide. After 10 min of incubation on ice, the lysate was centrifuged for 10 min at 12,000 g at 4°C. 1mg of protein extract was sedimented on continuous sucrose gradients (15–50%) for 2 h at 200,000 g at 4°C. The gradient was collected in pre-polysome and polysome fractions, and RNA was extracted using 2 volumes of Trizol.

Protein extracts and western blot analysis

Cell pellets were re-suspended in lysis buffer (50mM Tris-HCl pH 7.5, 0.5% Triton, 250mM NaCl, 50mM NaF, 1mM EDTA) supplemented with 2mM Na-orthovanadate, 1mM DTT and protease-inhibitors. Extracts were sonicated for 10 s and centrifuged for 10 min at 14,000 rpm, 4°C. Supernatants were quantified by Bradford assays, diluted in SDS-sample buffer, boiled for 5 min, and analyzed by western blot using the indicated primary antibodies. HRP-linked secondary antibodies were used. Secondary antibodies conjugated to horseradish peroxidase were incubated at 1:5000 dilution for 1 h. Immunostained bands were developed using Clarity Western ECL Blotting Substrate and Alliance Q9 Advanced imaging system.

Immunofluorescence assays

TNBC cells were fixed with 4% formaldehyde and permeabilized with 0.5% Triton X-100 in PBS. After 1 h of blocking whit PBS - 3% horse serum, cells were incubated over-night with anti-γH2AX (1:600) or anti-cyclin A (1:200) in blocking buffer. After rinsing, cells were stained for 1 h with secondary anti-mouse Alexa Fluor 594/anti-rabbit Alexa Fluor 488 antibodies (1:500). Nuclei were counterstained with 5 μg/ml Hoechst for 10 min. Immunofluorescence images were captured using a 100X objective of the Zeiss Axiophot fluorescence microscope.

For immunofluorescence of organoids, treated PDOs were washed with PBS and fixed with 500 μL of 4% paraformaldehyde for 30 min at room temperature. After three washes in PBS 1X, they were permeabilised in blocking solution (PBS, 0.5% Triton X-100, 5% horse serum) for 2 h. Subsequently, the organoids were incubated with anti-γH2AX antibody in blocking solution overnight at 4°C. Organoids were washed with PBS and stained with secondary anti-mouse Alexa Fluor 594 (1:500) overnight at 4°C, away from light. Then two washes were carried out in PBS for 10 min each and the third wash contained in 5 μg/ml Hoechst. Then, PDOs were re-suspended in PBS and arranged in the 8-well chamber slide (μ Slide 8 well, IBIDI, Cat#80806). For each organoid, the staining of the Z

plane with the highest fluorescence intensity was captured using a 100X objective under a Nikon Eclipse Ti2-inverted microscope. A minimum threshold of fluorescence intensity was chosen manually using ImageJ software for the γH2AX foci count.

Flow cytometric analysis of phosphorylated histone H2AX

MDA-MB-231 cells were harvested after indicated treatments fixing in cold 70% ethanol and stored at −20°C for up to two weeks before analysis. Cells were washed in Tris-buffered saline (TBS) and rehydrated for 10 min in TBS containing 3% BSA and 0.5% Tween 20. An equal number of cells were stained with anti-γH2AX antibody (1:200) in TBS containing 3% BSA over night at 4°C. After three washes with TBS, cells were incubated with secondary antibody Alexa Fluor 488 (1:400) for 1 h. Next, cells were re-suspended in TBS supplemented with 10 μg/mL RNase A and 2.5 μg/mL 7-AAD. A minimum of 10.000 stained cells were acquired on CytoFlex flow cytometer and analyzed using CytExpert software.

Cytofluorimetric sorting of MDA-MB-231 cells

Treated cells were fixed cells and stored in 70% ethanol for up 1 week. After washing with DPBS, 10^6 cells were stained with 1 mL of 20 μg/ml propidium iodide in DPBS supplemented with protease inhibitors and RNAsin (1:1000). After 30 min of incubation at 4°C in the dark, cells were sorted by DNA content in G1, S and G2/M phases of cell cycle using the BD FACSMelody sorter. The collected cells were centrifuged at 500 *g* for 10 min using a swing out rotor and lysed with 1% SDS in 50mM TrisHCl pH8.8. After decrosslinking at 95°C for 10 min, the samples were diluted in SDS-sample buffer and analyzed by western blot.

Immunohistochemical analysis

Five μm sections of paraffin-embedded tissues and HystoGel-embedded PDOs were stained using appropriate primary antibodies and the UltraView Universal DAB Detection Kit on the ULTRA instrument (Ventana) BenchMark. Appropriate positive and negative controls were included. The selected antibodies are well-established in the diagnostic routine laboratory, signals were clearly visible and captured by the Zeiss AxioPhot Microscope. Scores were performed by an expert pathologist.

QUANTIFICATION AND STATISTICAL ANALYSIS

Number of replicates, the standard deviation (SD), the standard error of mean (SEM) and the appropriate statistical test used for the analysis of every experiment is indicated in each figure legends. Analyses were performed in GraphPad Prism and p-value ≤ 0.05 was considered significant. For all tests, *,$,#: $p \leq 0.05$, **,$$,##: $p \leq 0.01$, ***,$$$,###: $p \leq 0.001$.